university of groningen / faculty of science and engineering

Energy harvesting possibilities with acoustic metamaterials

CmME

Master's research project

July 7, 2021

Student: Emre Özer

Primary supervisor: Dr. Anastasiia Krushynska

Secondary supervisor: Prof. Dr. Antonis Vakis

Acknowledgements

I would like to state my deepest gratitude toward the people that assisted me and walked with me through this journey.

To start with, I wish to thank my first supervisor, Dr. Anastasiia Krushynska for her continuous support and care during this period. The guidance I have received from her both accelerated my progress and provided a much deeper understanding. Thank you for all the advice that was not simply limited to an academic study.

Likewise, my sincere gratitude is also to my second supervisor, Prof. Dr. Antonis Vakis. Even though our meetings were less often, your feedback and support were very valuable.

I would like to especially thank Nitesh Anareo for the great collaboration through the project. It was a pleasure working with you. I wish we had time to finish what we started with the experimental setup, but still, I believe I learned a lot from your knowledge and experience on this. All of your help is greatly appreciated.

I am also grateful to the research group, Zhaohang Zhang and Bing Han. I have truly enjoyed our discussions about the papers on our weekly meetings and although our research areas are different to some extent, I am glad to be able to look to the field with a different perspective.

Last but not least, I would like to thank my parents for their guidance and wisdom at every point of my life, to my friends for their continuous support and especially to my girlfriend for being with me at every moment of my study, even through a distance.

Abstract

Manipulating acoustic waves, especially at low frequencies, has been a challenging task for engineers. Conventional materials are unable to provide sufficient sound isolation since signals with longer wavelengths require wider structures to achieve the desired absorption, which is often infeasible for many applications.

Acoustic metamaterials is an emerging research field that aims to design meta structures with specifically adjusted material parameters (i.e. negative effective density, negative effective bulk modulus etc.). As a result, the overall structure exhibits desired properties that allow advanced control over acoustic waves that can not be achieved with standard materials.

Even though acoustic waves do not carry a significant amount of energy, the wideness of application areas, such as sound absorbers near highways or airports, creates a possibility to generate a considerable supply of energy from low-frequency sound waves. This study aims to investigate the possibility of converting acoustic waves into electricity with means of acoustic metamaterials designed to attenuate low-frequency sound.

Table of Contents

List of Figures

List of Tables

Acronyms

AEH acoustic energy harvester. 2, 6, 13

HR Helmholtz resonator. 2, 4, 6, 8, 11–16, 18, 21–25, 31, 34–36, 40, 44, 52–54

MAM membrane-type acoustic metamaterial. 1, 10, 11, 15, 25, 36, 41, 52–54

PA perfect absorption. 2, 8, 9, 15, 53

PVDF Polyvinylidene fluoride. 15, 20, 32, 35, 39, 40, 49, 53, 54

SPL sound pressure level. 1, 25, 36

TL transmission loss. 2, 3, 10, 11, 25, 48

1. Introduction

Sound attenuation has been a deeply investigated subject for a long time. Acoustic noise that emanates from a device or an operation is generally considered disturbing and thus desired to be reduced or, if possible, eliminated. Conventional techniques such as the use of porous material or absorber walls to manipulate acoustic waves near highways, airports, industrial sites, power plants or other types of noise sources are widely being used.

The excess noise causes noise pollution, which is disturbing and even unhealthy to exposed individuals. Certain standards are being used to limit noise originating from commercial or industrial exploitation of devices. For instance, according to the standards of the Occupational Safety and Health Act (OSHA) introduced in 1970, the duration of exposure to high-level noise in workplaces must be limited, see Table 1.1.

Duration (hour per day)	**SPL (dBA)**
8	90
6	92
4	95
3	97
2	100
1.5	102
1	105
0.5	110
0.25	115

Table 1.1: Permissable noise exposures. (OSHA, 1970)[36]

According to the table, as the sound level increases the allowed exposure duration decreases severely, meaning that noise reduction is necessary for continuous operations. Yet these applications contain limitations due to the physical limitations of conventional materials, especially in a low-frequency range.

The elimination of noise offers a distinctive opportunity. The wave energy of noise that needs to be extracted from a medium can be harvested for beneficial usage. During the absorption process, the energy of an acoustic wave is typically transformed to heat and dissipates within the absorbing medium. A harvesting mechanism can be utilized to convert this energy into useful electric energy, resulting in an alternative energy source from sound.

Recent studies on acoustic metamaterials provided vast knowledge on controlling wave dynamics. These specifically designed structures extend the noise-damping techniques beyond the limitations mentioned. This work aims at the investigation of a new methodology for combined acoustic energy harvesting/attenuation purpose by means of membrane-type acoustic metamaterials (MAM) for predefined frequency ranges.

1.1 Metamaterials

The concept of dynamic metamaterials is based on the design of a material(or structure) to enable a specific property that can not be achieved with conventional materials or mechanisms[17]. Essentially, metamaterials can be categorized under composite structures. The distinctive characteristics of dynamic metamaterials are their ability to have unusual dynamic effective parameters and different behaviour under varying inputs. This is usually related to the frequency of an incident wave [34]. The dynamic effective parameters can have negative values in certain frequency ranges, which is impossible to achieve with conventional materials. The ability to tune the parameters according to the desired function enables the control over waves beyond natural limits [24].

1.1.1 Acoustic metamaterials

Dynamic metamaterials designed to manipulate sound waves are known as acoustic metamaterials. Usually consisted of periodic arrays, the macroscopic behaviour of the meta-structures depends on the properties of its local cells rather than the lattice itself [27]. The individual cells are generally smaller than the wavelength they affect. Such a structure enables control over acoustic waves with sub-wavelength elements [5]. The physics of these elements are defined by their effective material parameters. For applications in acoustics, effective bulk modulus and effective mass density hold a major importance [9].

Helmholtz resonators (HR) are a very common type of structure used in acoustic wave control. It is able to capture waves at a certain frequency and it can attenuate the acoustic energy at its resonance frequency. It is widely used in literature to provide perfect absorption PA [[31],[4],[1]], broadband absorption [[16],[19]] and energy harvesting purposes [[41],[27]]. Due to its ability to control and absorb acoustic waves at certain frequencies, it builds the base for the proposed system in this research.

1.1.2 Acoustic energy harvesters

Converting acoustic energy into electricity is studied deeply in the last few decades. It is possible to transform the energy of the sound wave to mechanical energy by using structures such as cantilever[33], membranes[22] or films[41], known as acoustic energy harvesters(AEH). The piezoelectric effect is used widely in these structures to generate electricity from the deformation of the structure caused by acoustic energy. Using a method similar to this, it is possible to convert the acoustic energy trapped inside a HR to electricity.

1.2 Problem definition

Within the context of classical materials, the sound absorption performance of a material or structure is described by the mass-density law which suggests that doubling the mass of the insulating element can only increase the transmission loss (TL) by approximately 6dB or quantitatively:

$$TL = 20 * \log f + 20 \log \rho_A - 47dB[40] \tag{1.1}$$

where f is the frequency of an incident sound wave and ρ_A is the surface density(mass per unit area) of an isolation element.

This leads to a complication that the amount of required mass (hence the volume) increases greatly to achieve a higher TL for conventional insulation solutions which would be hardly feasible or from the opposite point of view, as frequency decreases, the required mass increases resulting in a situation that low-frequency waves penetrate the insulating structure unless sufficient isolation is provided with large structures.

One other problem that will be stated in this research is the possibility of conversion of the absorbed acoustic energy into electric energy. In conventional isolation solutions, acoustic energy is absorbed by the material rather than being reflected or transmitted. This means that the energy of acoustic waves is transferred to the material, resulting in mechanical vibrations. These vibrations damp out in time, turning into heat. Hence, acoustic energy is converted into heat. It is logical to assume that this waste energy could be harvested.

There are various methods to convert acoustic wave energy into useful forms. The studies mentioned in Section 2 indicate several solutions. The main challenge with such a study is that acoustic waves carry low energy and therefore the acquirable energy can be insufficient for any kind of application.

In conclusion, these two problems can be summarized as follows

1. Attenuating low-frequency sound waves requires large structures made of conventional materials due to their poor attenuation performance. Utilizing such absorbers can be both economically and physically unfeasible. Alternative approaches are required to develop an absorber with smaller dimensions.

2. Acoustic waves do not carry a large amount of energy. Even though the generation process does not require an additional financial or physical input, since the usable energy is scant, it may not be possible to effectively utilize this energy.

This study aims to solve these two issues about low-frequency sound attenuation and acoustic energy harvesting. The scope of the study and the methodology are defined to address these problems.

1.3 Scope and methodology

The project intends to investigate the possibility of an energy harvesting mechanism while attenuating the noise, using acoustic metamaterials. However, the feasibility of a potential solution is not in the scope of interest. Therefore, the study will remain on a theoretical route rather than exploring real applications. The possibility of simultaneously harvesting and attenuating acoustic waves within a sub-frequency domain is the main topic of interest.

The proposed solution will consist of a combination of two isolation elements, Helmholtz resonators and a membrane-type acoustic metamaterial. A cross-section draft of the intended design is given in Figure 1.1a and the printed sample of this design can be seen in Figure 1.1b. The blue material represents the air inside the waveguide and the resonator. The green part is the piezoelectric membrane and the red part is the added mass to tune the resonance frequency of the system. The mass is attached to the membrane and the membrane is placed at the top of the resonator, replacing the rigid wall. The resonator has the ability to trap acoustic waves at its resonance frequency while a vibrating membrane is known to provide extreme wave control abilities [43]. The focus is on evaluating the attenuation performance of the coupled solution.

The energy harvesting possibility from vibrations of a membrane will be examined. For this purpose, piezoelectric materials are promising alternatives to convert mechanical energy to electricity. The vibration energy of a piezoelectric membrane can be used to generate energy in a similar way.

1.4 Research questions

Within the explained context and the defined problem, the goal of this research is to explore theoretical aspects of acoustic energy harvesting while achieving sufficient noise reduction by using meta-structures. The main research question is;

"How can membrane-type metamaterials be used to reduce structural dimensions and attenuate noise, concurrently generating energy from acoustic waves?"

In order to identify the study steps, the main research question is divided into sub-questions. Each of the sub-questions is designated to a specific step and finding the answers to the sub-questions will lead to the answer to the main research question.

1. **How does the tuning of Helmholtz resonators affect the attenuation frequency?**
   Increasing the stiffness or the inertia of a resonator-membrane coupled system results in variations of its resonance frequency. This also changes attenuation and energy harvesting. The establishing of the dependency of the varying tuning parameters will be the first milestone.

2. **How does the configuration of a HR affect the design and performance of the system?**
   Using single, dual or multiple resonators is an option to achieve the desired objective. These different configurations have different outputs in terms of attenuation and energy generation. Similarly, a hard-backed tube(closed-end) or anechoic tube(open end) also affects these properties. Thus, the design should be adjusted according to these conditions. Hence, the second milestone is defining the configurations and their impact on the target characteristics.

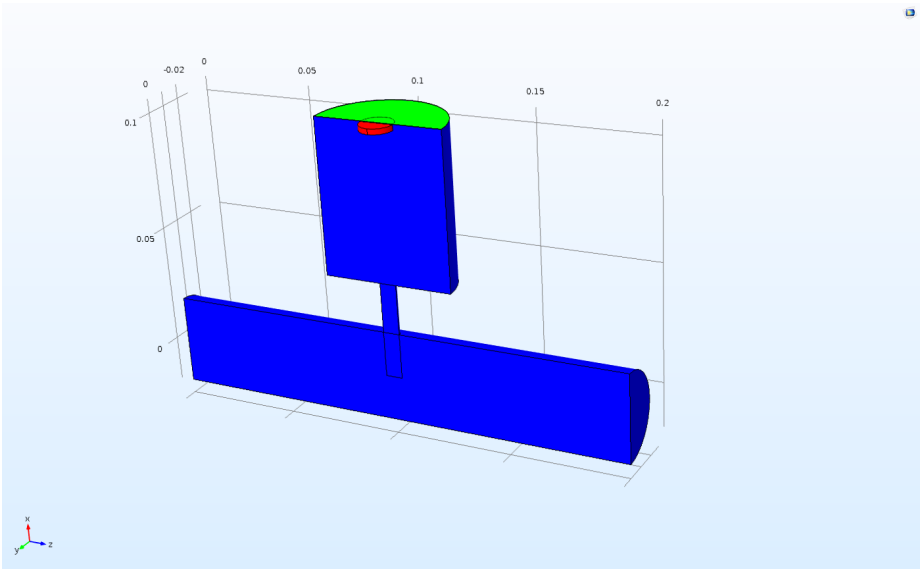

(a)

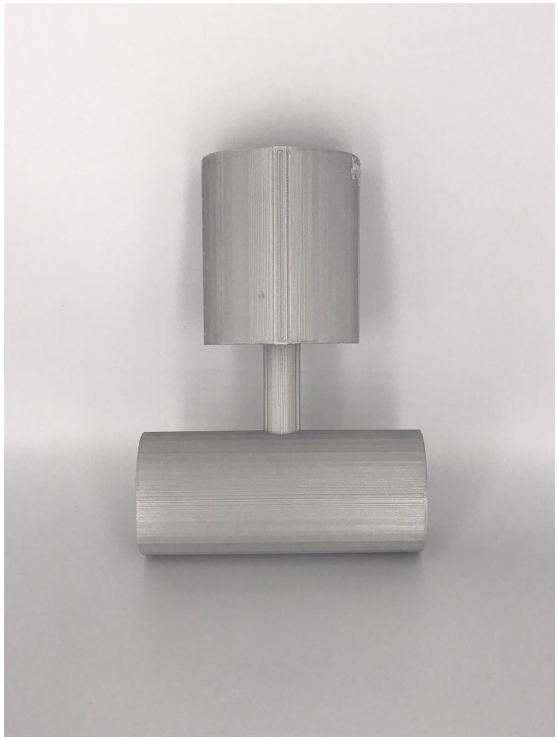

(b)

Figure 1.1: The proposed structure, (a) built in COMSOL and (b) manufactured by 3D printing.

3. **Does the energy harvesting process affect the efficiency of the noise reduction performance?**
   To achieve maximum noise reduction, critical coupling conditions are analysed. Since the initial goal is to increase the transmission loss, the energy output is estimated for the maximum sound attenuation. However, the effect of the energy harvesting system on noise reduction performance is a property of interest.

4. **What is the effect of the membrane elasticity on flow characteristics?**
   Using a membrane in a HR reduces the stiffness of a system, therefore affecting the flow. The pressure and velocity distribution within the waveguide can give valuable insight into the acoustic properties. Investigating these properties is helpful to understand the behaviour of a membrane coupled HR to enhance its design.

1.5 Structure of the thesis

Section 2 provides necessary background information about recent studies on acoustic metamaterials, AEH's and several different types of solutions addressing the aforementioned problems. The state-of-art studies in topics of acoustic metamaterials, sound attenuation and acoustic energy harvesting are demonstrated in this section.

Section 3 defines the research methodology and study steps to clarify the route taken to reach the research goal. The mathematical formulation of the problem, the solution steps and optimization procedures are explained in this section.

Section 4 explains and interprets the results obtained from the study. The efficiency of the proposed solution, comparison with different configurations are discussed.

Section 5 briefly summarizes the work done and the answers to the stated research questions. The limitations are explained in the section as well as the potential future work paths.

2. State-of-art literature

The field of acoustics, noise reduction and sound attenuation problems have been studied extensively. Energy harvesting through acoustic waves has also been considered by many researchers.

2.1 Metamaterials

The discovery of negative index materials dates back to the late 1960s. Victor Veselago conducted research on electromagnetic wave propagation in a special material, which is known as metamaterial today, proving the presence of negative effective indices is possible to be achieved. He also invented the term "left-handed materials" in his study by building an electromagnetic metamaterial with both negative permittivity and negative permeability [39]. However, the usage of metamaterials with the purpose of manipulating the acoustic waves became an attractive research area after Martînez-Sala et al. published a paper about the sound attenuation properties of a periodic hollow tube structure in 1995. The structure was a piece of art, a metallic sculpture placed in a park. The researchers discovered that the periodicity of the sculpture provided extreme sound attenuation properties, even though it was not intended to be [29].

2.2 Acoustic metamaterials

The field of acoustics has evolved significantly with the introduction of metamaterials. In this study, since two aspects are considered as the main focuses namely sound attenuation and energy harvesting, the reviewed studies are categorised according to their subject: about acoustic properties or about the energy harvesting mechanism.

2.2.1 Perfect absorption

Most of the studies investigating an advanced attenuation performance use periodic structures to exploit the local resonance of the cells. An example study for low-frequency sound attenuation was planned to be an array of plates placed on top of each other with cavities in between by Brooke et al. with the name of “pancake absorbers”. A representation of this structure is given in Figure 2.1. An analytical solution was found and validated through experiments. The material was able to provide an absorption coefficient up to 1 in both linear and nonlinear regimes of airflow [4].

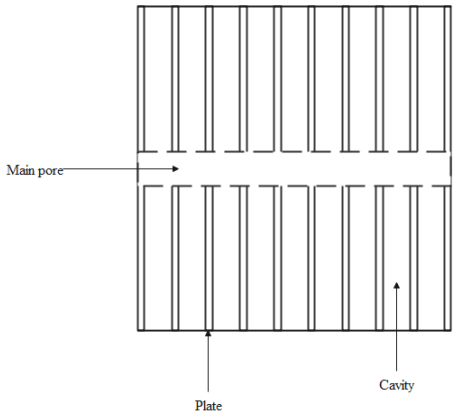

Figure 2.1: Pancake absorbers. Redrawn from [4].

Helmholtz resonators build the base of many studies in the field of acoustics and sound absorption and they are deeply studied for attenuation purposes. Achilleos et al. studied a single Helmholtz resonator attached to a tube to measure its absorption performance where both linear and nonlinear losses were taken into account. They were able to prove experimentally that, it is not possible to achieve more than 50% absorption with a single resonator [1].

A more generalized case was investigated by Merkel et al. and a similar result was found. In a study about resonant scatterers, they demonstrated that with symmetric structures, even in the critical coupling conditions a one-sided absorber can achieve a maximum of 50%. The term one-sided here refers to a hard-backed tube, meaning that the closed-end performs as a perfect reflector. In the same study, it was also proven that asymmetric structures are able to provide absorption rates of over 90% in a one-sided absorber [30]. The maximum of absorption in one-sided(one-port, closed-end) resonators can be expressed quantitatively by;

$$A = 4\frac{C_{leak} * C_{loss}}{(C_{leak} + C_{loss})^2}, \tag{2.1}$$

where "leak" subscript indicates the radiation leakage and "loss" subscript indicates intrinsic losses, both with a unit of kg/s [35] [20]. It can be deduced from the equation that the maximum attenuation can reach a value of 1 when $C_{leak} = C_{loss}$, indicating the critical coupling.

In general, two factors affect the ability to reach PA: whether the resonator is a single port or two-port and whether if it's symmetric or not. The potential solutions are categorized as a two-sided tube with a single resonator, a one-sided tube with a single resonator, a two-sided tube with two symmetric resonators and a two-sided tube with two detuned resonators. In the first case, the maximum absorption is 0.5 and at the maximum of absorption, the transmission and reflection coefficients are 0.25 and equal due to the radiation symmetry [30][1] [20]. In the second case where a single resonator is placed in a tube with a closed-end, the reflected waves from the closed end of the tube can cancel the reflected waves from the resonator, resulting in a destructive interface to

achieve PA. In this case, the resonator must be placed a distance of quarter wavelength of the resonance frequency away from the end of the tube($d \approx \lambda/4$). The third case fails to achieve PA due to the symmetry. [30] [20] However if the symmetry is broken, the radiating waves from each resonator would be able to cancel each other, resulting in PA. In conclusion, the system has to be either one-sided(single port) or it has to be two-sided(two-port) that contains a dual resonance [20]. A schematic representation of these conditions can be seen in Figure 2.2.

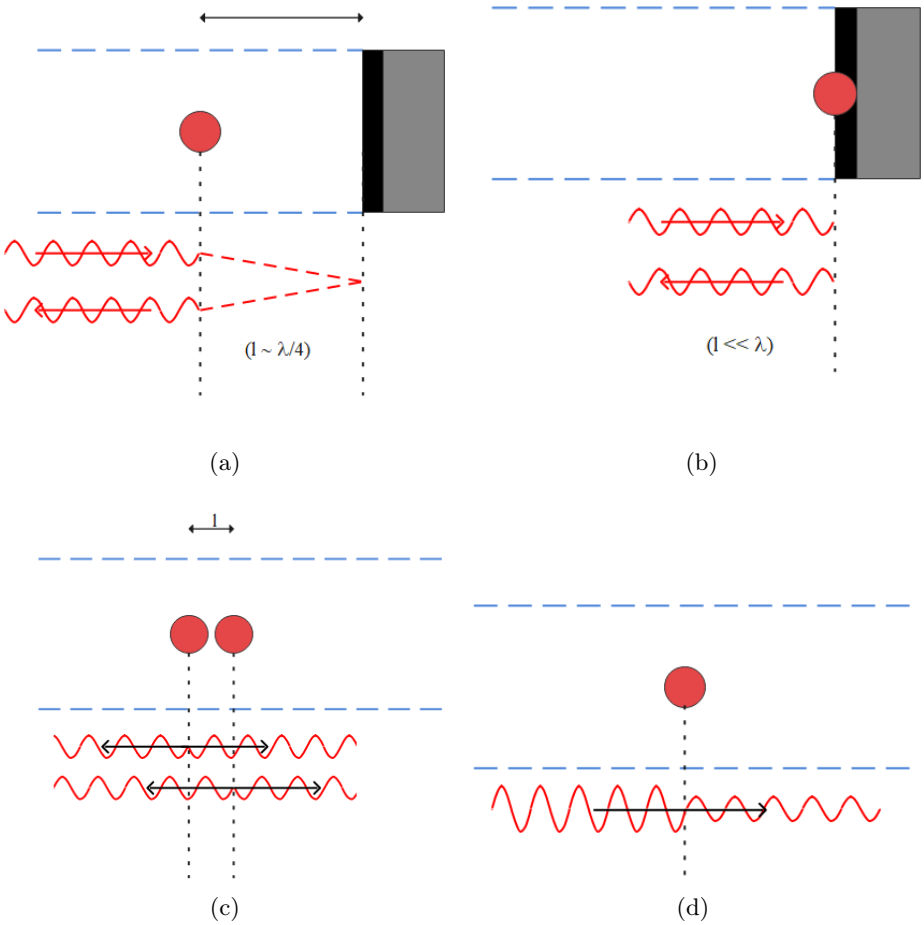

Figure 2.2: (a) Single resonance resonator in one-port system placed away from the reflector, (b) single resonance resonator in one-port system placed on the reflector, (c) dual resonance resonator in two-port system and (d) single resonance resonator in two-port system. Redrawn from [20].

Another factor that affects systems with multiple resonators is the distance in between. Using two resonators means adding another degree of freedom to the system. If it is a two-port system, perfect absorption can be achieved by keeping the distance between the resonators shorter than the quarter wavelength($d \ll \lambda/4$) [20] [11]. However, it should also be noted that the largest attenuation band can be achieved by keeping the distance at half-

wavelength($d \approx \lambda/2$) [11]. It is possible to find an optimum solution for both achieving high attenuation and large bandwidth, yet it is not in the scope of this study thus, it will not be discussed further. According to the study conducted by Gautam et al. in the case of a quarter wavelength separation, the pressure distribution is out of phase between the resonators, meaning that while one resonator is having a maximum, the other one has a minimum. The experimental study suggests that the first resonator, in this case, is responsible for the high attenuation peak while the second one provides an increased bandwidth of attenuation. On the other hand, while the separation is half of the wavelength, the resonators are in phase. This configuration results in larger bandwidth attenuation in both resonators, causing the largest bandwidth, yet, the maximum attenuation is lower than the previous configuration [11].

Another milestone for acoustic metamaterial study can be referred to as the study of Huang, Hu and Sun about membrane-type acoustic metamaterials coupled with mass. After modelling the vibroacoustic characteristics of a membrane analytically, the difference in eigenmodes and sound transmission with an added mass on the membrane was studied. The study discovered that presence of a central mass shifts the eigenfrequency of the mass-membrane system to lower frequencies while providing a dramatic drop of sound transmission between the first two eigenmodes. The study also suggests that by adding an eccentricity to the position of the mass, it is possible to tune the MAM and change the TL peaks [43]. The placement of the membrane in the tube and the mass on the membrane is given in Figure 2.3.

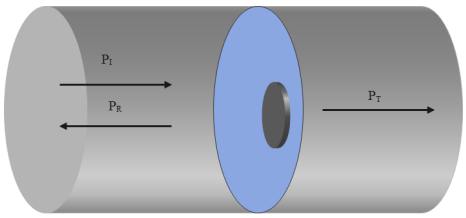

Figure 2.3: Mass coupled membrane absorber. Redrawn from [43].

Another mass-membrane coupling was used in a study by Lu et al. where a MAM with eccentric masses was designed for sound isolation. Attenuation performance and range of a square membrane with a ring mass was investigated in the study and it was found out that depending on the parameters such as membrane thickness, pretension or mass configuration, it was possible to obtain TL peaks of 20dB within the range of 50-250 Hz [28].

It is also possible to build an asymmetric resonator system with membrane resonators decorated with mass. By using a degenerate membrane resonator, Yang et al. achieved perfect absorption in their study. A single decorated membrane resonator and a coupled one were attached to a panel, creating perfect absorption. The particle velocity distribution in the study shows how the system achieves 99% absorption. The velocity is towards the resonators on the inlet side, but on the outlet side, the particles are moving away from the single resonator, towards the coupled resonator, creating 0 velocities at outlet [42].

Mi and Yu used a MAM in a 'U' shaped tube to couple two HRs. The two ends of the tube were connected via a bridge with 2 identical coupled Helmholtz resonators that are separated by a membrane. Analytical and finite element solutions are used for validation and it was determined that a TL up to 50dB was achievable within the regime of 100-600 Hz [31]. The configuration of this system and the structure of the HR used in this system is given in Figures 2.4a and 2.4b.

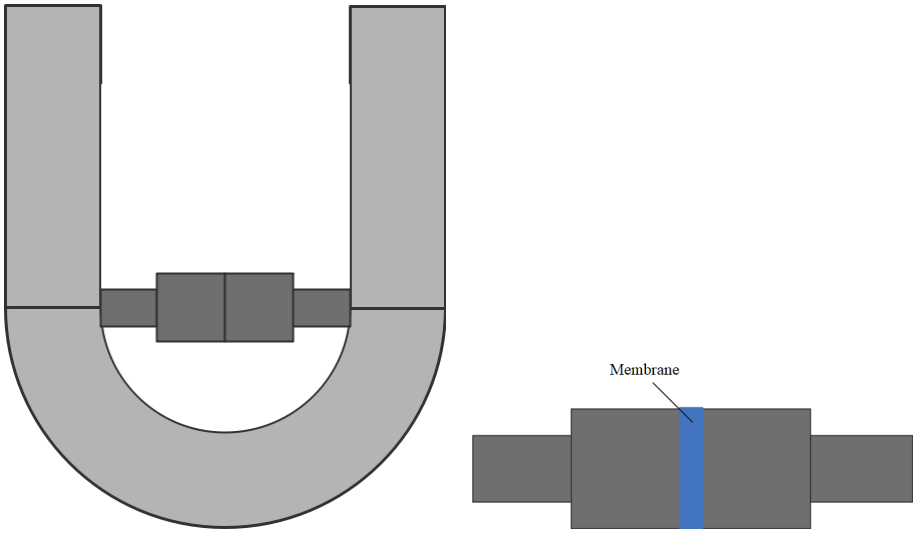

(a) (b)

Figure 2.4: The geometries of the (a) U shaped tube and (b) the HR bridge between two ends of the tube. Redrawn from [31].

The analytical solution to the physics of the MAM was derived by Langfeldt et al. to calculate the TL with rectangular and circular membranes. The results were then compared to the finite element solution for validation [18].

The usage of elasticity was investigated by other scientists too as Cui et al. proposed a soft material based resonator to achieve almost absolute absorption of acoustic waves. The system is basically achieved by replacing the walls of the resonator with elastic materials and adjusting the structure according to that. Several aspects were investigated in the study along with the difference between the soft and the rigid HR. The first topic was the effect of the opening radius. It was observed that almost 90% absorption was possible in a low-frequency regime with smaller openings (3 mm) and several peaks of absorption were identified in larger openings (5 mm). Material properties were also in the area of interest. The effect of Young's modulus and wall thickness interaction on the absorption coefficient was also investigated. In conclusion, it was observed that the soft materials enable absorption in multiple frequencies, Young's modulus of the material adjusts the bandwidth of the absorbed frequency and the dimensions can be adjusted to tune the resonator similar to simple HR's [8].

2.2.2 Broadband absorption

Even though HR's are effective in sound absorption applications, the major drawback is that they work in a narrow band [20]. In real applications, a single, narrow attenuation peak is very likely to be considered adequate. It is possible to increase the bandwidth of attenuation or to tune the system to operate at the desired frequency.

One way to increase the bandwidth is to use "Rainbow Trapping Absorbers" as defined by Jimenez et al. which is a panel, decorated with an array of 8 nonidentical Helmholtz resonators. The asymmetry of the resonators results in slightly different resonance frequencies. By coupling those resonators, it is possible to increase the attenuation bandwidth of the overall system. The study of Jimenez et al. demonstrated that an attenuation band of approximately 100 Hz was achieved with two coupled resonators, 200 Hz with three resonators and a band of approximately 700 Hz was achieved with 8 coupled resonators. The panel has a size of 10x3 cm, between 10% and 30% of the frequency band [16]. A representation of this design is shown below.

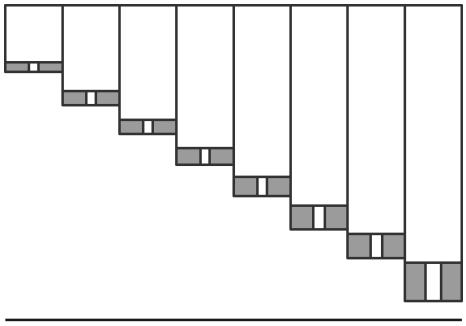

Figure 2.5: Rainbow-trapping absorber. Redrawn from [16].

Rather than achieving broadband absorption, a simpler solution is to tune the peak attenuation frequency to the desired level. In a Helmholtz resonator, the resonance frequency can be adjusted by changing the effective stiffness(the volume of the cavity) or by changing the effective mass(the volume of the neck) [13]. For example, Lee et al. proposed a tubular array of Helmholtz resonators to freely adjust the working frequency range. The volumes of the resonators are controlled by plungers, moving towards or away from the resonator to change the cavity volume, adjusting the resonance frequency [19]. Figure 2.6 demonstrates the working principle of this system.

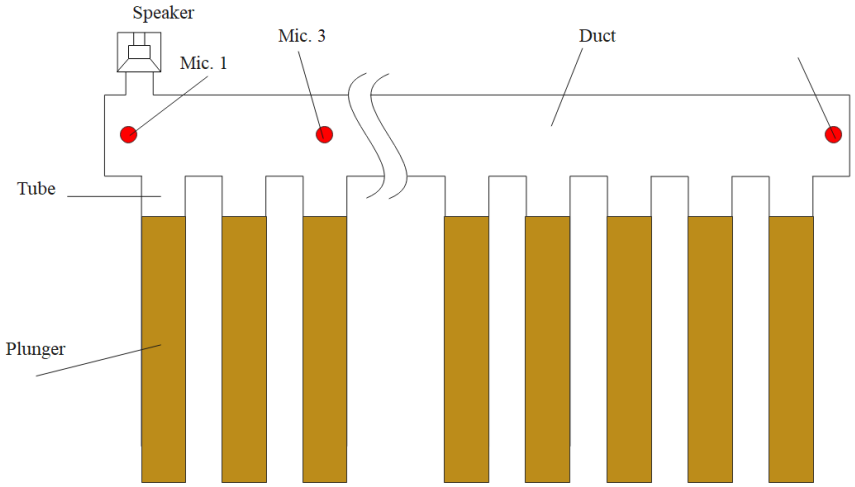

Figure 2.6: Highly tunable resonator. Redrawn from [19].

The development of membrane absorbers led scientists to investigate the applicability of the solution in various conditions. Liu and Du investigated the tuning properties of membrane-type acoustic metamaterials. In their study, the researchers used strip masses attached to a membrane that is planted on the sidewalls of a rectangular tube. The mode shapes of the membrane and the strip masses were examined and the effect tuning parameters on peak frequencies such as eccentricity of the mass, number of masses and weight were explained to enable the fine adjustment of the insulator [26].

2.3 Acoustic energy harvesting

Converting acoustic energy to electrical energy is a subject of interest for a long time. A MEMS(Microelectromechanical system) based AEH was proposed by Horowitz et al. in a study in 2005 where the circuit was used with a piezoelectric ring inside a HR. Two energy peaks were observed in the simulations, one for the resonance of the resonator and one for the eigenfrequency of the harvesting mechanism [15].

An example study to harvest energy from low-frequency sound waves was conducted by Li et al. in 2013. In the study, the group used piezoelectric cantilevers composed of polyvinylidene fluoride to harvest the acoustic energy in a quarter wavelength resonator. The experiments were done for single cantilever and multiple cantilevers. The cantilevers were designed to have an eigenfrequency equal to the excitation frequency, which is the first eigenmode of the resonator in order to maximize the energy output of the proposed system. The experiments were done with a sound wave of 100dB with a 146Hz frequency. The study investigates several aspects; the position inside the resonator to place the cantilever, the number of cantilevers and the placement order of cantilever beams(straight line and zigzag configuration) that maximize the energy output were investigated. The results suggested that 9 piezoelectric cantilevers, ordered

in a zigzag configuration in the first half of the resonator provided the maximum voltage output [21].

Another harvesting mechanism was proposed by Pillai et al. in 2014 where they used a Helmholtz resonator with a tapered neck and a PVDF cantilever to harvest the acoustic energy at the resonance frequency of the HR. The resonator was designed to have a resonance frequency of 284 Hz and the cantilever was designed to have the same eigenfrequency. The system was excited with an incident wave of 95 dB. During the experiments, an output voltage of 396 mV was observed [33].

Guang-Sheng Liu et al. built an array of coupled Helmholtz resonators through an elastic membrane to generate power from a wide frequency range of sound waves. In the study, adjacent resonators with rectangular cross-sections were coupled by changing the mutual walls of the adjacent resonators with piezoelectric membranes. The resonators are adjusted to have different resonance frequencies, causing a phase difference between two resonators which is used to vibrate the membrane to harvest the acoustic energy. This structure can be seen in Figure 2.7 [25].

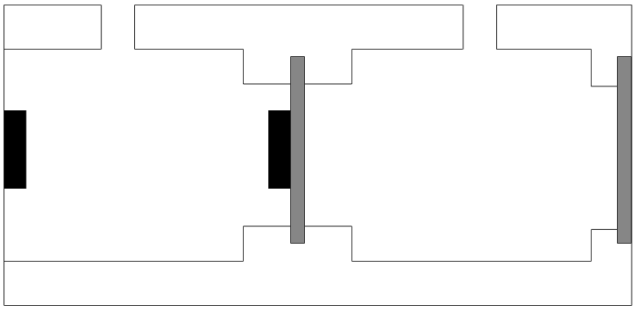

Figure 2.7: Membrane coupled-resonator array for acoustic energy harvesting. Redrawn from [25].

Wang et al. proposed a real application of simultaneous sound attenuation and acoustic energy harvesting in 2018 by using noise barriers that are composed of arrays of HRs, containing piezoelectric films in their cavities to prevent the transmission of the noise and to convert the acoustic energy to electricity. The study was able to achieve up to 50 mV at 500 Hz. The proposed sound barriers were designed to be used near high-speed railways [41].

Li et al. proposed a structure that is capable of providing large transmission loss as well as converting acoustic energy into electricity. The research used the structure from [43] as the base and changed the membrane material to a thin piezoelectric film to generate energy with displacement. The mass is used to tune the membrane. The sound attenuation performance of the study was similar to the study by Huang et al. but the power generated from the system is limited to a level of nano-watts [22].

3. Methodology

To achieve the goal introduced in Section 1.2 we need to specify a geometry that is capable of both attenuating the wave energy and transforming it to amplified mechanical vibrations with the aim to harvest the energy through piezoelectric materials. For this purpose, HRs are excellent candidates to amplify the wave energy at their resonance frequency and are also widely used as sound absorbers due to their high absorption coefficient at these frequencies [14], [32]. The trapped and amplified waves can be transferred into mechanical vibrations and eventually to electricity, using PVDF films.

The task is to tune the eigenfrequency of a Polyvinylidene fluoride film to match the resonance frequency of a HR. The MAM proposed by Yangyang et al. [43] will be taken as a reference point to adjust the natural frequency of the PVDF film.

3.1 Mathematical formulation

The basic element of the structure is represented in Figure 1.1a. The basic element is built by a mass-loaded membrane coupled HR attached to a tube. The acoustic wave enters the system through the inlet of the tube. The waves with a frequency equal to the HR frequency are trapped inside the cavity of the HR. The acoustic pressure in the resonator causes the elastic membrane to vibrate and the membrane generates electricity due to the piezoelectric effect. The piezoelectric film is connected to a circuit for further usage such as storing the electricity or directly using it.

However, several modifications are required on this basic element to achieve the desired functions. The first step to build the model is to construct the geometries for the system. Two alternative solutions are inspected at this stage: two-port and one-port systems.

Two-port system contains two resonators attached to a tube with an open end, providing anechoic termination. One-port system has a single resonator and a closed end, assumed to be a perfect reflector. As explained by Lee et al. [20] one-port system can achieve PA by placing a HR at a distance of $d = \lambda/4$ from the perfect reflector. In a two-port system, two resonators are required to reach PA. Those two resonators should be slightly de-tuned and separated by a distance of $d \ll \lambda/4$. Conducting an analysis on two alternatives can provide sufficient information to answer research questions 2 and 3. Thus, two models are constructed: a single resonator-closed end tube and dual resonators-open end tube. The section view of these two systems are given in Figures 3.1a and 3.1b.

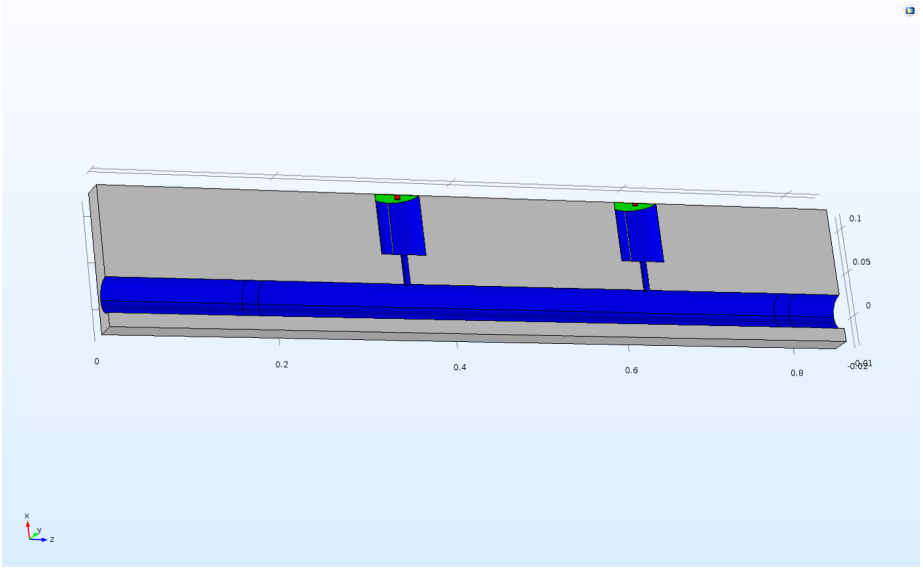

(a)

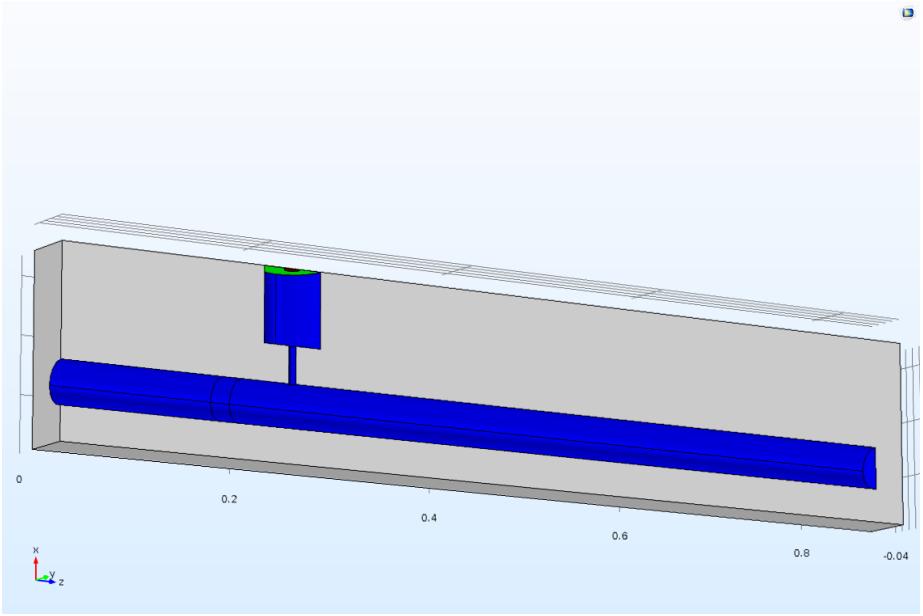

(b)

Figure 3.1: Sectional views of geometries for the proposed (a) two-port and (b) one-port systems.

The green domain is the membrane with the attached red mass. The blue areas represent the air inside the HR and the tube. The grey part is the material of the proposed system.

To express the problem mathematically, we start from investigating the pres-

sure distribution in the tube. First we define the effective compressibility and effective density of air as functions of frequency. Stinson's study on generalization of plane sound waves in tubes (1990) is used to calculate the these parameters for a circular tube [38], which are given by equations (3.1) and (3.2), respectively:

$$\rho(\omega) = \frac{\rho_0}{1 - \frac{2}{\sqrt{\frac{-iw}{v}}} \times \frac{J_1(r_w * \sqrt{\frac{-iw}{v}})}{r_w * J_0(r_w * \sqrt{\frac{-iw}{v}})}}, \tag{3.1}$$

$$C(\omega) = \frac{1}{\gamma P_0} * \left(1 + \frac{2(\gamma - 1)}{\sqrt{\frac{-iw\gamma}{v}}} \times \frac{J_1(r_w * \sqrt{\frac{-iw\gamma}{v}})}{r_w * J_0(r_w * \sqrt{\frac{-iw\gamma}{v}})}\right). \tag{3.2}$$

The parameters ω, J_n and r_w in the equations are the angular frequency of the incident wave, Bessel function of order n and the radius of the tube, respectively. The equivalent bulk modulus of air, used in the model is the inverse of the equivalent compressibility, (3.2).

Knowing the effective bulk modulus(K_e) and density (ρ_e), one can calculate the effective speed of sound in the tube:

$$c_e = \sqrt{\frac{K_e}{\rho_e}} \tag{3.3}$$

and the corresponding wave number:

$$k_e = \frac{\omega}{c_e}^2 \tag{3.4}$$

The pressure distribution in the tube then can be represented mathematically by equation (3.5).

$$p_b = p_0 * e^{-i * k_e * \frac{r \cdot e_k}{\|e_k\|}}, \tag{3.5}$$

where p_0 is the amplitude of the background pressure, r is the spatial coordinate and e_k is the incident wave direction.

The boundary conditions for this step are the sound hard boundary walls for the inner walls of the structure shown in Figure 3.1 and plane wave radiation boundaries to the open ends of the tubes. Those conditions are expressed mathematically by equations (3.6) and (3.7)[12], respectively.

$$-n \cdot \left(-\frac{1}{\rho_c}(\nabla p_t - q_d)\right) = 0, \tag{3.6}$$

$$-n \cdot \left(-\frac{1}{\rho_c}(\nabla p_t - q_d)\right) + i\frac{k}{\rho_c}p + \frac{i}{2k\rho_c}\nabla_T p = \frac{i}{2k\rho_c}\nabla_T p_i + i\frac{k}{\rho_c}p_i + n \cdot \frac{1}{\rho_c}\nabla p_i. \tag{3.7}$$

Equation (3.6) indicates that the normal component of acceleration at the given boundaries is 0. The wave only propagates through the air, not through the material. Equation (3.7) expresses the reflected wave from the surface. The reflection decreases with the angle of the surface to the normal vector of the

wave, meaning that the reflection is zero for normally incident waves [12].

The HR locally modifies the pressure distribution in the tube. Transmission, reflection and attenuation properties of the tube are indeed greatly affected with the presence of a HR. Thus, it is essential to tune the HR to achieve the desired acoustic properties. Since the maximum absorption occurs at a resonance frequency of the resonator, the first step is to identify this frequency. In a HR, the air inside the cavity is considered to be compressible but when the volume of air in the neck is relatively smaller compared to the cavity, it can be considered as incompressible. The compressible air inside the cavity acts as a spring while the incompressible air in the neck vibrates as a mass. This assumption enables the modelling of a HR as a mass-spring system with the air in the neck being the mass and the air in the cavity is the spring. The resonance frequency is given by the equation (3.8) [7] :

$$f_H = \frac{c}{2\pi}\sqrt{\frac{A}{V_0 L_{eq}}}, \tag{3.8}$$

where c is the speed of sound, A is the equivalent area of the neck, V_0 is the static volume of the cavity and L_{eq} is the equivalent length of the neck. The equivalent length and the equivalent area of the neck are calculated by equations (3.9) and (3.10) [23].

$$L_{eq} = L + 0.6 * R_{neck}, \tag{3.9}$$

$$A = \frac{V_n}{L_e q} \tag{3.10}$$

with V_n being the volume of air in the neck.

The next step is to study the vibrations of the membrane. The membrane is attached to the top of the HR, replacing the rigid wall on top. Geometry and the placement of the membrane are shown in Figure 3.2. The green domain is the membrane and the red domain is the attached mass. The blue part shows the inside of the HR. The pressure inside the HR causes displacement on the membrane. The basic approach to the solid mechanics problem is given by Equation (3.11),

$$0 = \nabla \cdot S + F_v, \tag{3.11}$$

where ∇S is the divergence of stress and F_v is the volume force on the membrane.

The boundary conditions for this problem are the fixed constraints on the side walls of the membrane (3.12), preventing in-plane displacements and initial stress on the membrane surface (3.13).

$$u = 0, \tag{3.12}$$

$$S = S_0, \tag{3.13}$$

where S_0 is the initial stress matrix.

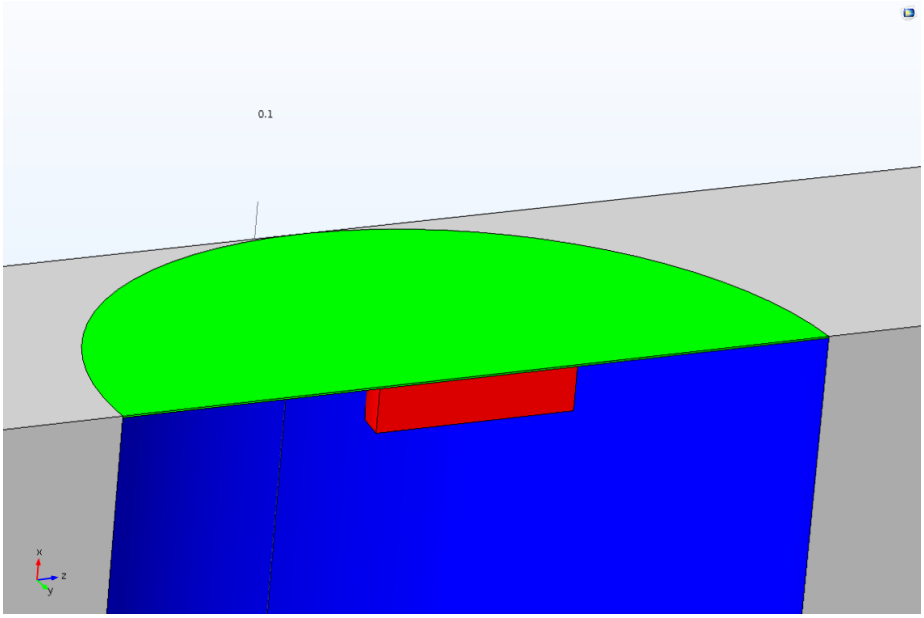

Figure 3.2: Placement of the membrane.

Calculating the vibration frequency of the membrane is also necessary to tune the membrane frequency to match the Helmholtz resonator frequency. Natural frequencies of the membrane can be calculated by equation (3.14) [3].

$$f_m = \frac{\alpha_{ij}}{2 * \pi * R} \sqrt{\frac{F}{t * \rho_m}}. \tag{3.14}$$

Here R is the radius of the membrane, t is the thickness, ρ_m is the material density, F is the surface tension force and α_{ij} is a parameter used to calculate the frequencies of higher modes of vibration which takes the positive root of the Bessel function for the corresponding eigenfrequency as its value. Its value for the first two modes are $\alpha_{10} = 2.4048$ and $\alpha_{20} = 5.5201$.

The acoustic pressure causes out-of-plane deformation on the membrane. The volume of the cavity changes with the deformation of the membrane, affecting the pressure. This multiphysics coupling problem is defined by Equations (3.15) and (3.16), defining the acoustic pressure acting on the membrane and the resulting pressure from the displacement of the membrane.

$$F_A = p_t n, \tag{3.15}$$

where p_t is the total acoustic pressure, F_A is the load experienced by the structure and n is the normal vector of the surface.

The modified pressure field with the displacement of the membrane is expressed as;

$$-n \cdot \left(-\frac{1}{\rho_c} (\nabla p_t - q_d) \right) = -n \cdot u_{tt}, \tag{3.16}$$

where ρ_c is the density of air, q_d is given as the dipole source and u_{tt} is the structural acceleration.

The final task is solving the piezoelectric energy generation. The membrane is built from Polyvinylidene fluoride and a deformation creates charge imbalance, generating electricity. The governing equations for the electrostatic problem and piezoelectric charge conversion are as follows;

$$E = -\nabla V, \tag{3.17}$$

$$\nabla \cdot D = \rho_v, \tag{3.18}$$

where V is the dependent variable, electric potential, D is the electric displacement and ρ_v is the charge density. The effective strain on the membrane is calculated by (3.19),

$$\epsilon = \frac{1}{2}\left[(\nabla u)^T + \nabla u + (\nabla u)^T \nabla u\right], \tag{3.19}$$

while the electric displacement is solved by (3.20),

$$D = D_r + e\epsilon_{el} + \epsilon_{0,vac}(\epsilon_{rS} + JC^{-1} - I)E, \tag{3.20}$$

and

$$e = dS_E^{-1} \tag{3.21}$$

where d is the element of the coupling matrix and S_E is the element of the compliance matrix. e_{rS} is the relative permittivity and ϵ_0 is the initial strain on the membrane. The initial strain can be found from initial stress by using Equations (3.22) and (3.23),

$$\epsilon = S_E T + d^T E, \tag{3.22}$$

and

$$D = dT + e|rSE, \tag{3.23}$$

where T is the stress and E is the electric field.

The boundary conditions for this problem are a ground node for one side of the membrane ($V = 0$) and a floating potential for the other side as expressed in Equation (3.24),

$$\int_{\delta\Omega} D \cdot n dS = Q_0. \tag{3.24}$$

3.2 Numerical modelling

The problem is solved numerically by the means of the commercial finite-element software COMSOL Multiphysics 5.5 with Pressure acoustics, Solid mechanics and Electrostatics modules. Two type of physics coupling is necessary to consider: acoustic-structure coupling and structural-electrostatic coupling. A step-by-step approach was adopted to understand the physical process and to minimize unnecessary complifications at earlier steps. The physics of the three way interaction will be considered separately, then merged in smaller groups and finally, in a complete model.

3.2.1 Acoustic model

The structures that are analysed in this section are shown in Figures 3.1a and 3.1b. However, building the solid material of the system (grey domain) causes computational complexities that are unnecessary to consider. The boundary between the air and the system is assumed to be sound hard, meaning that the resonator and tube material has no influence on the computation. To reduce the computational complexity of the problem, the resonator and tube material is not modelled in COMSOL. The air inside the resonator, the membrane and the mass are the geometries constructed in COMSOL. The representation for there two models are given in Figures 3.3a and 3.3b.

A background pressure field is defined along the axis of the tube. For each section of the tube and the resonator with a different radius, a pressure module is defined to define the thermoviscous losses.

For the single port system, the tube has a single HR attached and the only difference is the outlet boundary condition, which is a closed-end in this case so defined as a sound hard boundary.

The physical properties of air that are necessary to implement to the model are given in Table 3.1.

ρ	1.2044[kg/m^3]	Density of air at T_0
c	343 [m/s]	Speed of sound in air
η	1.8140e-5 [Pa*s]	Dynamic viscosity at T_0
γ	1.4	Specific heat ratio
P_0	1 [atm]	Absolute pressure
T_0	293.15 [K]	Temperature
C_p	1005.4 [J/(kg*K)]	Heat capacity at constant pressure
k_t	0.025768 [W/(m*K)]	Thermal conductivity

Table 3.1: Physical properties of air.

Two additional parameters to be used, the bulk modulus of air and the Prandtl number, are expressed by equations (3.25) and (3.26).

$$K_0 = \gamma * P_0 = 1.4186e5Pa, \tag{3.25}$$

$$Pr = \eta * C_p/k_t = 0.70778. \tag{3.26}$$

The COMSOL interface does not include thermoviscous losses by default. The losses must be either modelled by defining the boundary layer for the flow, which would require many elements and increase the computational complexity severely or must be introduced manually by adjusting material parameters for air. Effective density and effective bulk modulus can be used at this step to define the losses. Effective density is expressed with Equation (3.1) and effective bulk modulus is the inverse of the effective compressibility expressed in Equation (3.2).

The next step is to determine transmission and reflection coefficients and introduce losses to calculate absorption. It is possible to calculate these values

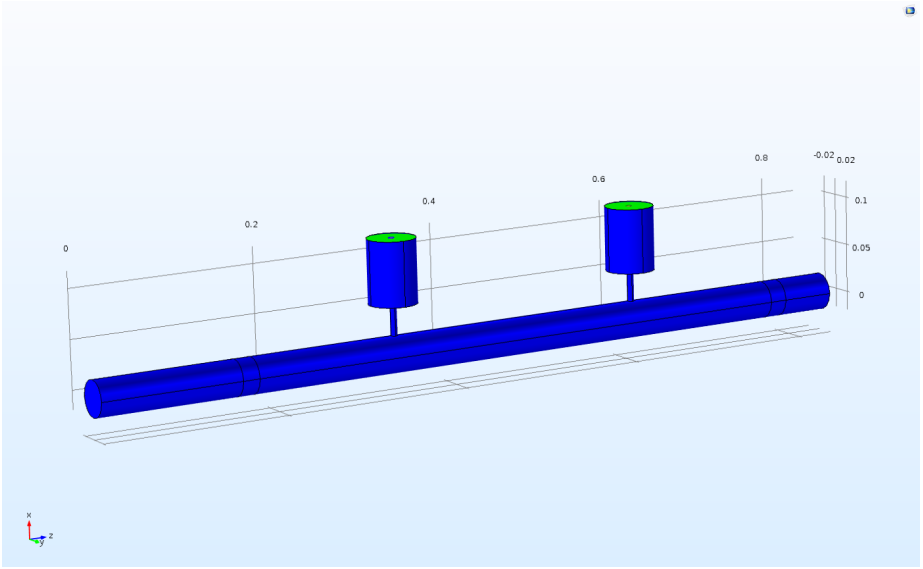

(a)

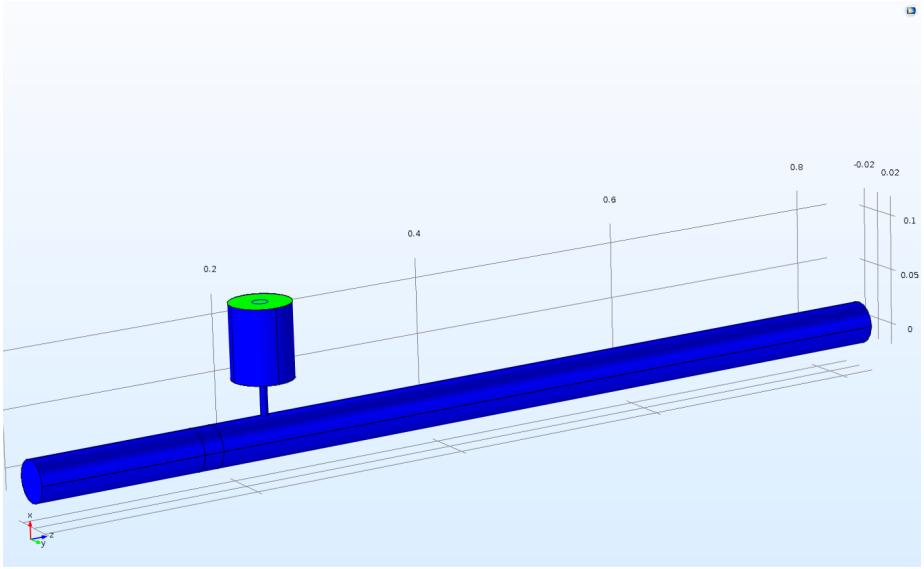

(b)

Figure 3.3: Geometry of the numerical model. (a) The two-port system: an open-end tube with two HRs. (b) The one-port system: a closed-end tube with a single HR.

experimentally by placing 4 microphones inside the tube and taking measurements from the upstream and downstream sides of the HR [10][37]. This experimental setup is shown in Figure 3.4 for an open-end tube. The setup for a closed-end tube is the same except the termination is hard-backed, acting as a reflector and the two microphones on the downstream side is redundant so only

two microphones are used.

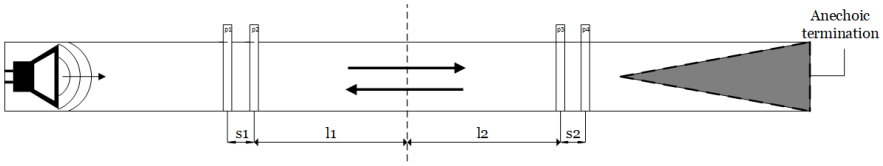

Figure 3.4: Experimental scheme of the open-end tube for tranmission and reflection measurements.

This experimental setup can be simulated in COMSOL environment by using pressure probes at certain points in the tube. The pressure values are named as $P_{1..4}$, with P_1 estimated at the closest point to the inlet and P_4 referring to the pressure at the closest point to the outlet for the two-port system. For the closed-end tube, the two points are between the inlet and the resonator. P_1 is the point close to the inlet and P_2 is the point closer to HR. The representation of this method is shown in Figure 3.5.

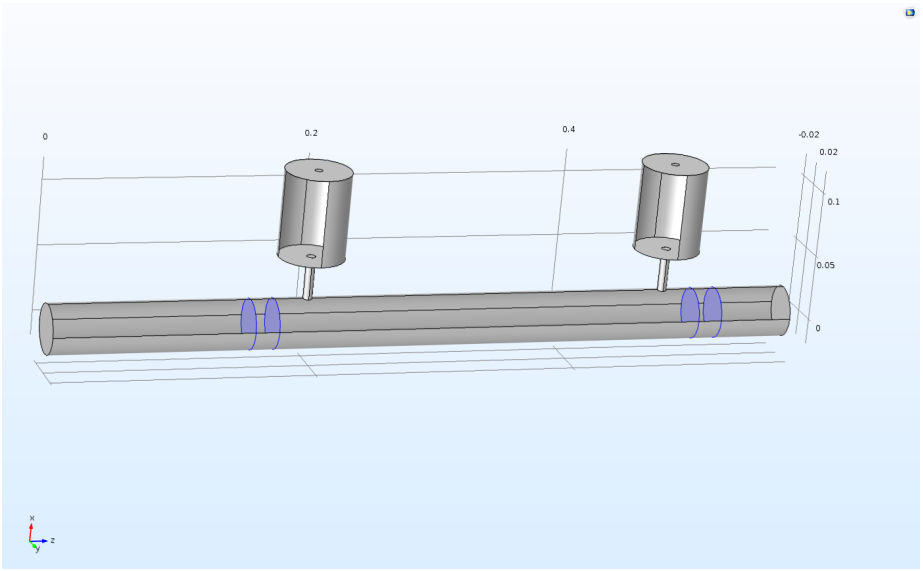

Figure 3.5: Pressure measurement points in the open-end tube.

For the placement of the probes, the standards of ASTM were used as guidelines [2]. The standard indicates several important aspects regarding the placement. Those are listed below:

- The upper limit for a working frequency is defined by equation (3.27).

$$f_u = \frac{Kc}{d}, \tag{3.27}$$

  where c is the speed of sound, d is the tube diameter and K is a constant equal to 0.586.

- The distance between the sound source and the closest probe must be three times larger than the tube diameter.
- Increasing the distance between two probes (s_n) enhances accuracy.
- The distance between two probes must not be larger than half wavelength of the upper-frequency limit, (3.27).
- The lower frequency limit is determined according to the purpose of the analysis while ensuring that the following condition is satisfied.
- The distance between two probes must be larger than 1% at the wavelength of the lower frequency limit.

The formula for the reflection coefficients for two and one-port systems is given by Equation (3.28) and transmission coefficient for two-port system by Equation (3.29) [10][37]:

$$R = \frac{p_1 * e^{ikl_1} - p_2 * e^{ik(l_1+s_1)}}{p_2 * e^{-ik(l_1+s_1)} - p_1 * e^{-ikl_1}}, \tag{3.28}$$

$$T = \frac{\sin(ks_1)}{\sin(ks_2)} * \frac{p_3 * e^{iks_2} - p_4}{p_1 - p_2 * e^{-iks_1}} * e^{ik(l_1+l_2)} \tag{3.29}$$

with variable k indicating the wave number. Parameters l_1, l_2, s_1 and s_2 are dimensions from the impedance tube, which are demonstrated in Figure 3.4. The blue disks represent points $P_{1..4}$. The distances between the points are s_1 and s_2 in the equations. The parameters l_1 and l_2 are the distance from the point to the position of the HR.

With the reflection and transmission coefficients, the absorption coefficient can be calculated for the two-port system with Equation 3.30 and for the one-port system with Equation 3.31.

$$A = 1 - |R|^2 - |T|^2, \tag{3.30}$$

$$A = 1 - |R|^2. \tag{3.31}$$

The goal is to reach the critical coupling conditions for the system at a sub-wavelength scale. The starting point is a validated design to ensure the accuracy of the methodology. The mirror-symmetric scatterer from the study of Merkel et al. [30] is used as a base geometry for the two-port system. The resonators in the single-port and two-port systems are initially identical. Their parameters are given in Table 3.2.

Neck radius	1 [cm]
Neck length	1 [cm]
Resonator radius	2.15 [cm]
Resonator length	4 [cm]

Table 3.2: The geometric parameters of the HRs.

The structural differences between one-port and two-port systems are in the placement of the resonators and the length of the tube. These data are given in Table 3.3.

Waveguide radius	5 [cm]
Waveguide length	80 [cm]
Two-port resonator 1 position	32 [cm]
Two-port resonator 2 position	62 [cm]
One-port resonator position	47 [cm]

Table 3.3: Tube dimensions for the two-port and one-port systems.

The pressure measurement points and the distances between the points are selected according to ASTM standarts as in Table 3.4. Additionally, the upper frequency limit is 4019 Hz and the lower frequency limit is 170 Hz according to the standarts.

Distance from inlet	20 [cm]
$l_1 = l_2$	30 [cm]
$s_1 = s_2$	1.8 [cm]
Distance to termination	5.5 [cm]

Table 3.4: Measurement point distances.

With the given parameters, the calculated resonance frequency of the HR is 645 Hz with Equation 3.8. The wavelength at this frequency is 0.53 meters. The results agree with the findings from the aforementioned study. The reflection and transmission coefficients for two-port and one-port systems are given in Figures 3.6a and 3.6b for a range of 300 - 950 Hz. The acoustic pressure and SPL for both models are shown in Figures 3.7a, 3.7b, 3.8a and 3.8b, respectively. Since the two-port system would also transmit the incidence waves, it is necessary to calculate the transmission loss (TL). The related plot is given in Figure 3.7c. It can be seen that the two HRs ensure a TL of ≈ 60 dB at the resonance frequency.

Diameter of the tube, resonator, neck; length of the neck, resonator and the distance between two resonators are the parameters to be adjusted to match the frequency of the HR to the frequency of the MAM. The resonators are planned to be identical and fine-tuning of the system is done through the MAM rather than the resonator.

The parameter list for the one-port and two port systems after the adjustments are given in Table 3.5 as well as the acoustic pressure, SPL and TL plots for the corresponding systems in Figures 3.9 and 3.10.

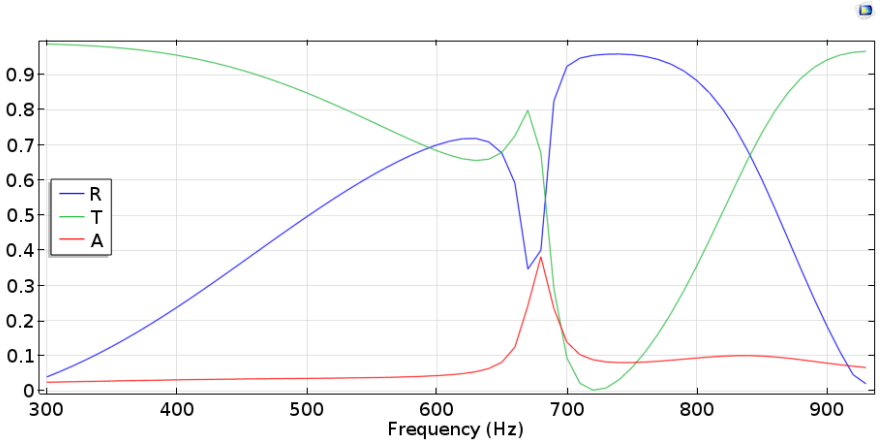

(a)

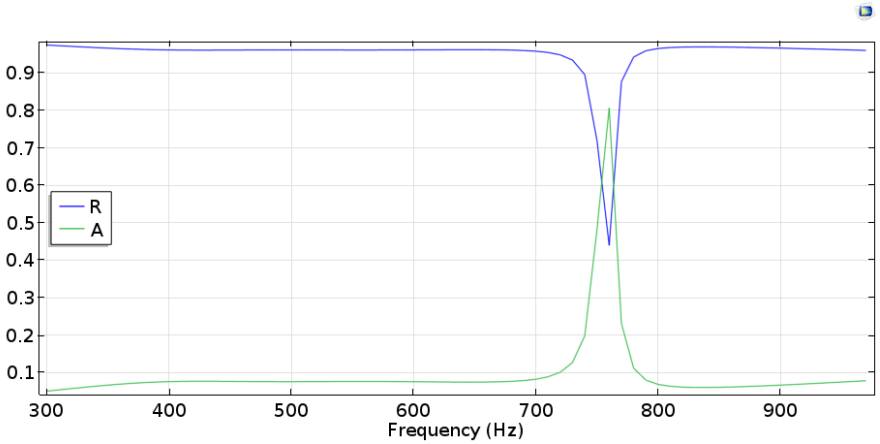

(b)

Figure 3.6: (a) Transmission, reflection and absorption coefficients for the initial two-port system. (b) Reflection and absorption coefficient for the initial one-port system.

Waveguide radius	1.9 [cm]
Neck radius	0.35 [cm]
Neck length	3.3 [cm]
Resonator radius	2.75 [cm]
Resonator length	6.6 [cm]
Position of the first resonator (two-port)	32[cm]
Distance between resonators (two-port)	27 [cm]
Position of the resonator (one-port)	22[cm]

Table 3.5: Adjusted dimensions for the two-port and one-port systems.

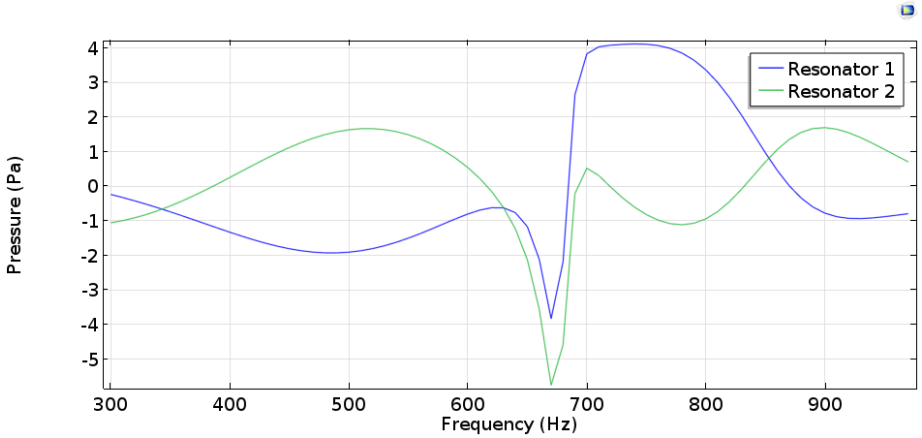

(a)

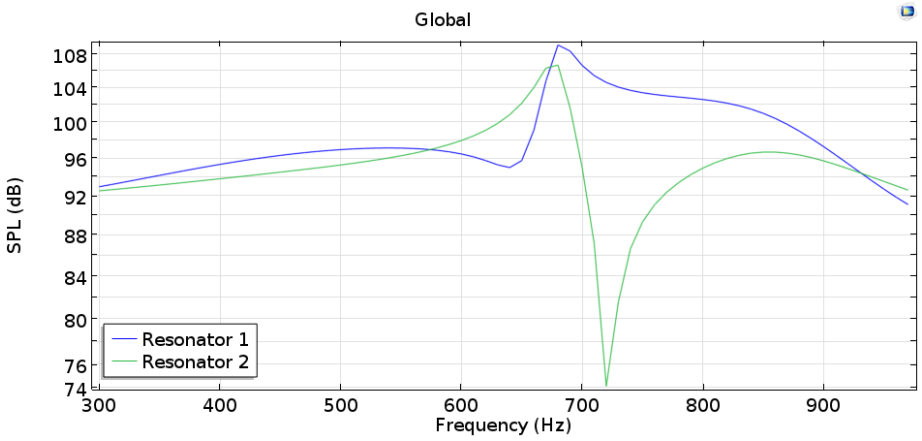

(b)

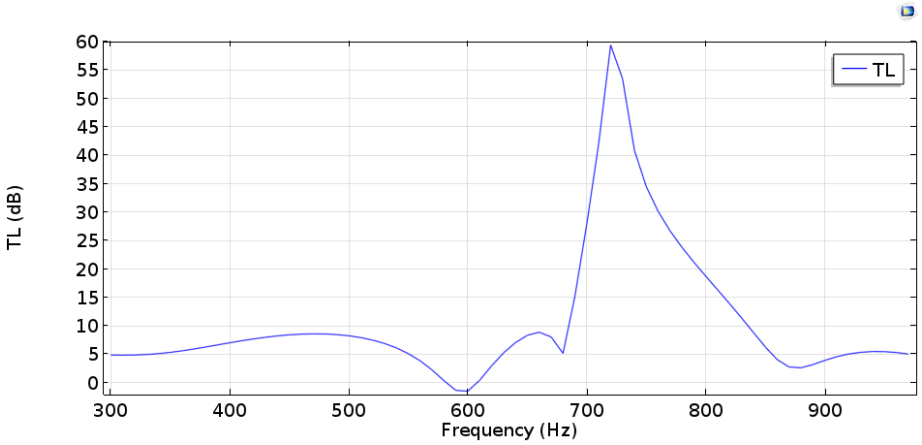

(c)

Figure 3.7: Acoustic properties with respect to the incident frequency for the initial two-port system. (a) Acoustic pressure and (b) SPL and (c) the corresponding TL.

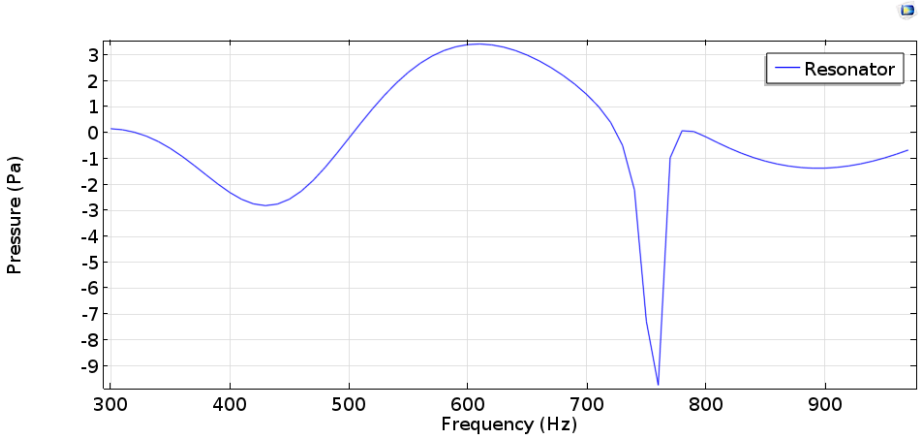

(a)

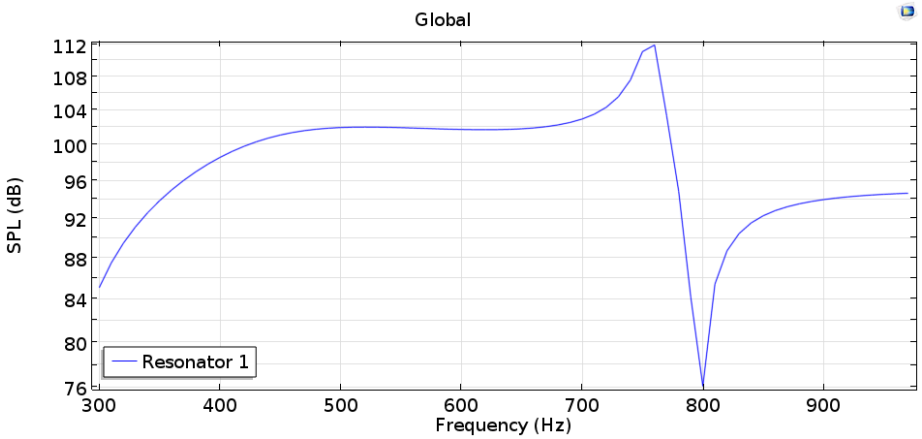

(b)

Figure 3.8: Acoustic properties with incident frequency for the initial one-port system. (a) Acoustic pressure and (b) SPL.

The correspinding reflection, transmission and absorption plots for the adjusted two-port and one-port systems are given in Figures 3.11a and 3.11b.

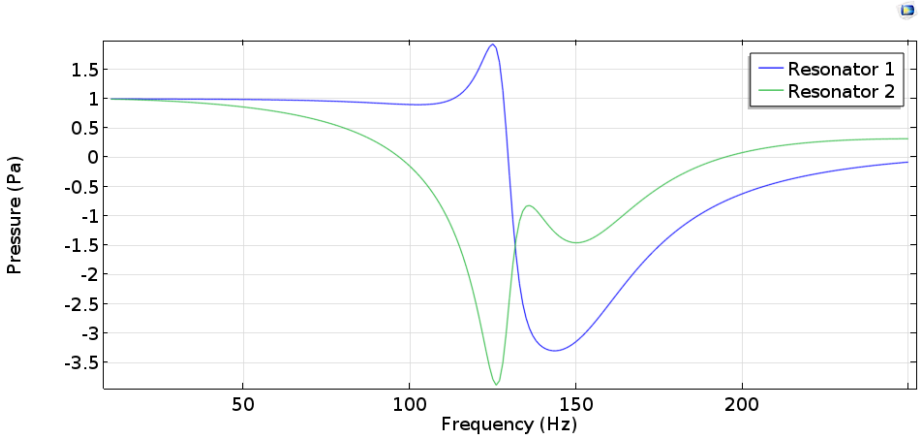

(a)

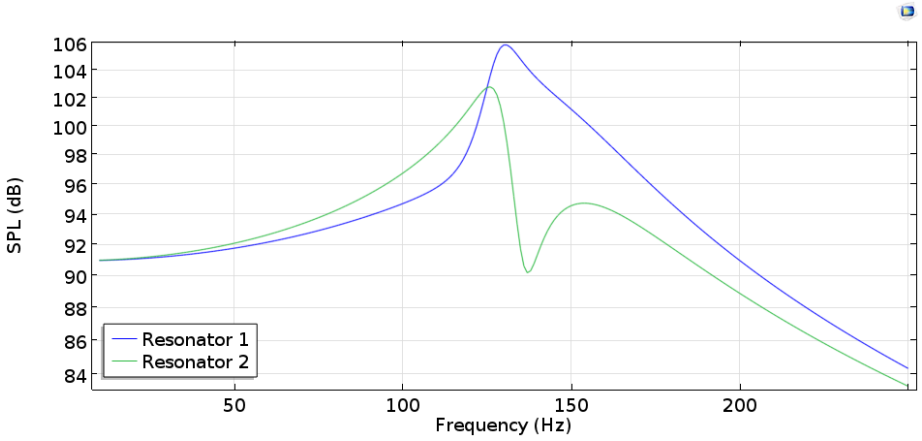

(b)

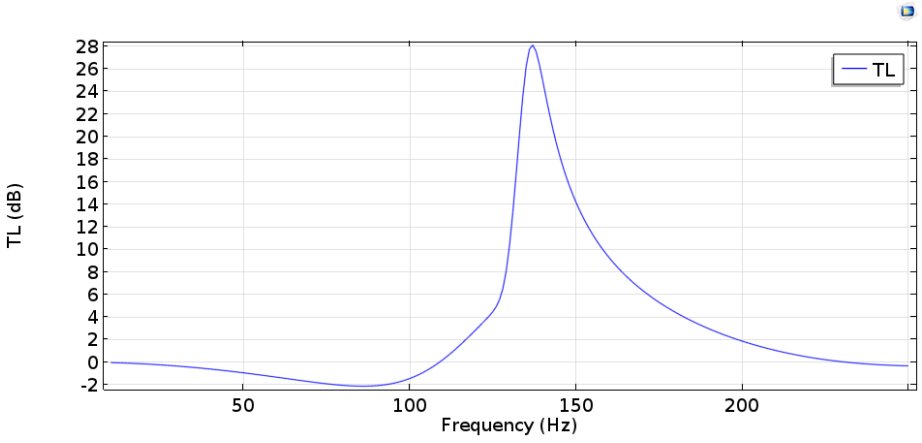

(c)

Figure 3.9: Acoustic properties with respect to the incident frequency for the adjusted two-port system. (a) Acoustic pressure and (b) SPL and (c) the corresponding TL.

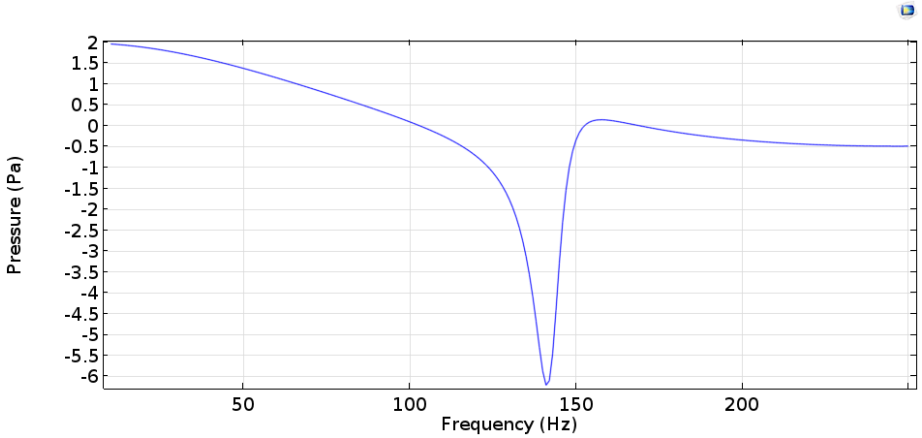

(a)

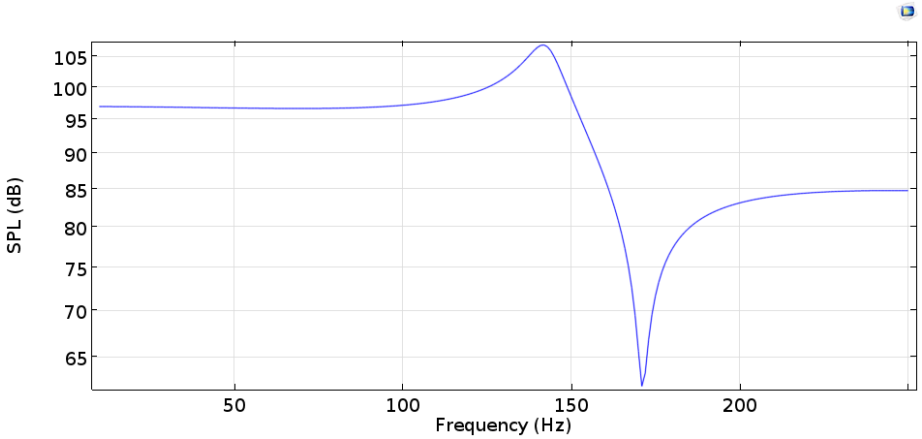

(b)

Figure 3.10: Acoustic properties with incident frequency for the adjusted one-port system. (a) Acoustic pressure and (b) SPL.

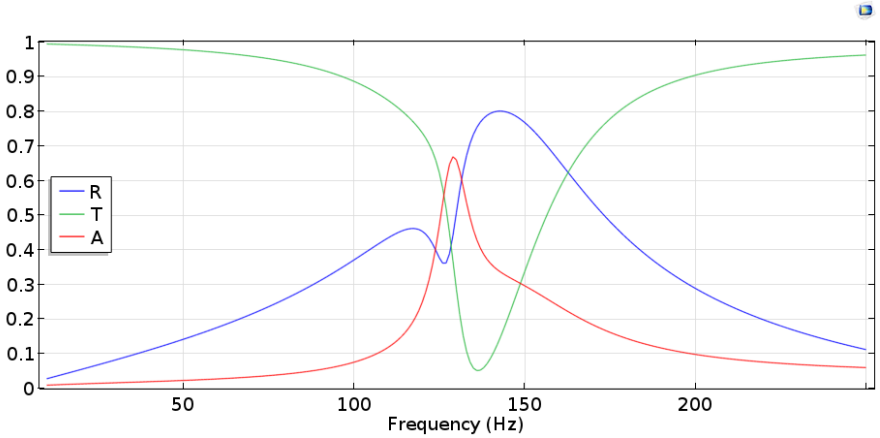

(a)

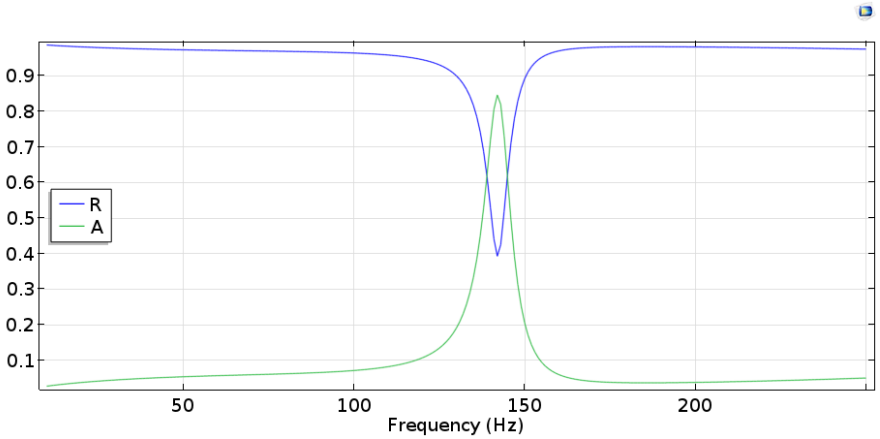

(b)

Figure 3.11: (a) Reflection, transmission and absorpiton coefficients for the adjusted two port system. (b) Reflection and absorpiton coefficients for the adjusted one-port system.

3.2.2 Analysis of structural vibrations of a membrane

The membrane has two functions in our systems: to improve the tunability as explained with the example studies in Section 2 and to generate power through piezoelectric effect. Therefore, the rigid end of the HR is replaced with a thin membrane to enable these functions. Geometry of this membrane is represented in Figure 3.12.

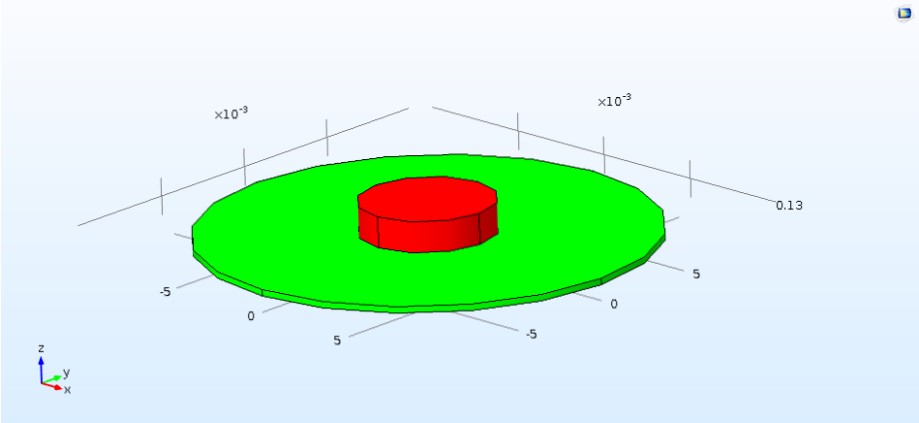

Figure 3.12: Geometry of the MAM.

Structural mechanics module of COMSOL Multiphysics is used to analyse the membrane vibrations. The membrane is attached to the upper end of the resonator with fixed constraints on the outer boundaries of the membrane the membrane is arranged to be a piezoelectric domain with initial in-plane stress.

Similar to the study on acoustics, the starting point for modelling the membrane is a geometry from a validated study. The membrane-type acoustic metamaterial used in the study of Chen et al. [43] is taken as an initial model and modified according to the purposes. The dimensions of the mass and the membrane are given in Table 3.6.

Membrane radius	1 [cm]
Mass radius	3 [mm]
Membrane thickness	280 [um]
Mass thickness	1.36 [mm]

Table 3.6: Dimensions for the membrane-mass model.

The material of the membrane is polyvinylidene fluoride(PVDF) and steel for the mass. The mass has Young's modulus of 200 GPa and a Poisson's ratio of 0.33 while the membrane has a Poisson's ratio of 0.49 and the elasticity of the PVDF is given as a default material parameter in COMSOL with the compliance matrix with (3.32).

$$S_E = \begin{bmatrix} 4.43e-010[1/Pa] & -9.91e-011[1/Pa] & -3.10e-010[1/Pa] & 0 & 0 & 0 \\ -9.91e-011[1/Pa] & 5.04e-10[1/Pa] & -3.19e-010[1/Pa] & 0 & 0 & 0 \\ -3.10e-010[1/Pa] & -3.19e-010[1/Pa] & 1.14e-9[1/Pa] & 0 & 0 & 0 \\ 0 & 0 & 0 & 1.82e-09[1/Pa] & 0 & 0 \\ 0 & 0 & 0 & 0 & 1.70e-09[1/Pa] & 0 \\ 0 & 0 & 0 & 0 & 0 & 1.45e-09[1/Pa] \end{bmatrix} \tag{3.32}$$

The last parameter for the study is the prestress on the membrane. Initial stress of 51.2 N/m is applied on the membrane in the planar direction. With the given parameters and Equation (3.14), the first two eigenfrequencies of the membrane without the mass is calculated as 523 Hz and 1200 Hz. The numerical solution of this problem suggests eigenfrequencies of 529 Hz (Figure 3.13a) and 1216 Hz (Figure 3.13b), in agreement with the analytical solution.

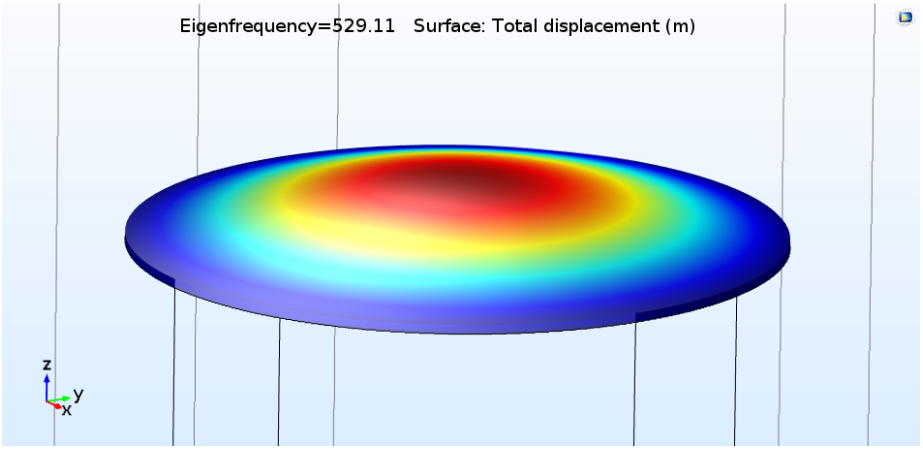

(a) First mode.

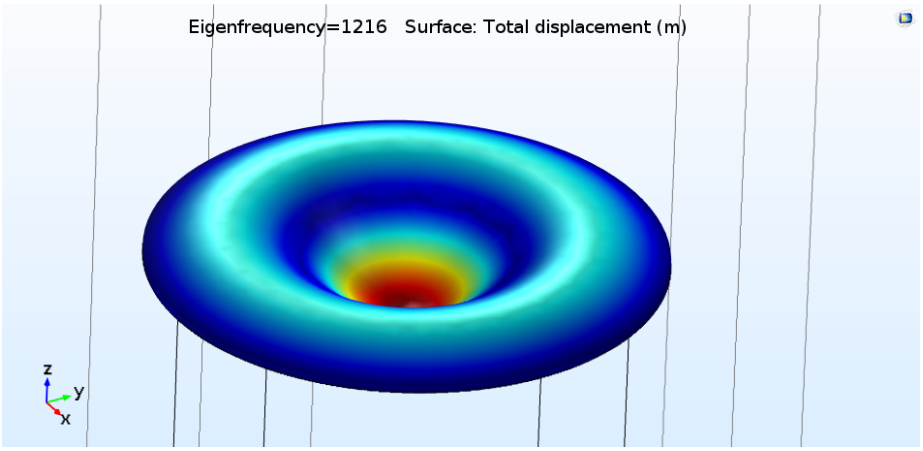

(b) Second mode.

Figure 3.13: The first two vibration modes of a membrane.

The colour map represents the out of plane displacement as red indicating the maximum of the displacement and blue representing the minimum displacement.

Attaching the mass has a major influence on the vibration frequencies of the membrane. The computed eigenfrequencies for the first two mode of the mass-loaded membrane are 148 Hz (Figure 3.14a) and 1004 Hz (Figure 3.14b), showing excellent agreement with the aforementioned study [43].

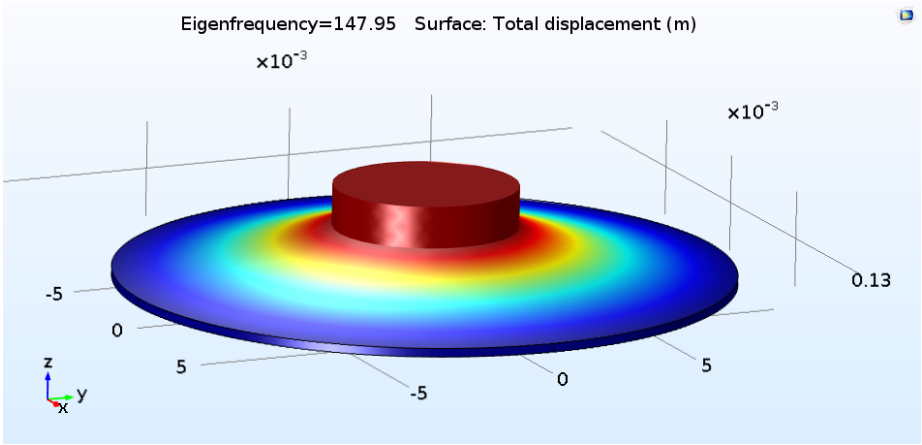

(a)

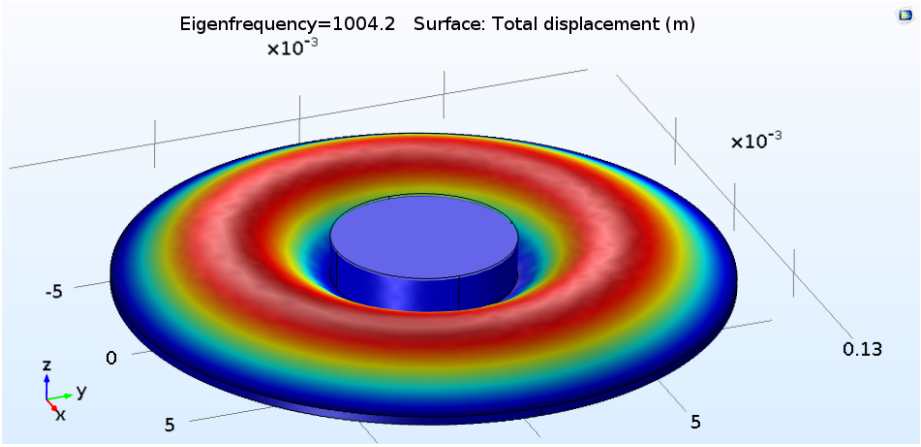

(b)

Figure 3.14: The first two modes of a membrane vibration with an added mass at the center.

Since the membrane is attached to the resonator, its diameter must be equal to the HR. In addition, the vibration frequency of the membrane is desired to match the HR frequency to increase the power output by enabling larger deformations on the membrane. Thus, its dimensions are adjusted to provide the desired properties. The adjusted dimensions for the membrane are given in Table 3.7.

Membrane radius	2.75 [cm]
Membrane thickness	80 [μm]
Tension	220 [N/m]
Mass radius	0.3 [cm]
Mass weight	0.1 [g]
1st natural frequency	143 [Hz]
2nd natural frequency	481 [Hz]

Table 3.7: Adjusted dimensions for the MAM.

3.2.3 Electrostatics

To convert the acoustic energy into electric form a PVDF film is used. Modelling piezoelectric effects in COMSOL requires coupling of the electrostatics module with the structural mechanics module. Hence defining the electrostatics is an essential step to build the coupling conditions.

The boundary conditions of the electrostatics problem are a ground boundary on the outer side of the membrane and a floating potential on the inner face of the membrane. A piezoelectric charge conversion domain is applied to the membrane.

The optimization of the harvesting mechanism is not within the scope of this research as mentioned, therefore, the material parameters are taken directly from the material library of the software. Those standard parameters are listed in Table 3.8.

ρ	1780 [kg/m^3]	Density
ϵ_r	6.8	Relative permittivity, xx
ϵ_r	8.4	Relative permittivity, yy
ϵ_r	7.3	Relative permittivity, zz

Table 3.8: Material parameters for the PVDF.

The coupling matrix to express the piezoelectric effect is give in (3.33).

$$d = \begin{bmatrix} d_{xx} \\ d_{yy} \\ d_{zz} \\ d_{yz} \\ d_{xz} \\ d_{xy} \end{bmatrix} = \begin{bmatrix} 1.36E-011[C/N] \\ 1.94E-011[C/N] \\ 2.97E-011[C/N] \\ 2.01E-011[C/N \\ 1.93E-011[C/N] \\ 0[C/N] \end{bmatrix} \tag{3.33}$$

3.2.4 Acoustic - structural coupling

The coupling problem is handled by using the membrane defined in section 3.2.2 with the acoustic problem defined in section 3.2.1. The membrane is attached to the close end of the HR and excited by the acoustic pressure inside the cavity. The attenuation performance, as well as membrane displacement at resonance,

is being investigated at this stage.

The only difference between the HR with membrane model from the simple HR (Section 3.2.1) is, the closed end of the resonator is replaced with a membrane that has an attached central mass.

The boundary conditions for both the pressure acoustics and structural mechanics parts of the problem is identical with those in the sections 3.2.1 and 3.2.2.
The acoustic-structure interface is defined on the face of the membrane that contacts the pressure field in the HR. The frequency-domain analysis was done in the range of 10-250 Hz.

The coupling increases the elasticity in the HR and the stiffness of the membrane. This results in a decreased frequency of HR and increased vibration frequency of the membrane. The displacement of the membrane with respect to frequency is represented in Figures 3.15a and 3.15b, showing the maximum point of the displacement at 97 Hz and 105 Hz for open-end and closed-end tubes, respectively. The pressure distribution and SPL in the resonators with the MAM attached is given in Figure 3.16 and 3.17.

Figure 3.16a shows that the resonators work out of phase at the resonant frequency. The slight difference in the resonant frequency can also be seen since the first resonator has a maximum at 100 Hz and the second resonator has a maximum at 96 Hz. The difference can also be observed in Figure 3.16b, where the de-tuning caused a slight shift on the maximum point of the SPLs.

For the closed-end tube, the resonance frequency is shifted from 140 Hz as calculated in Section 3.2.1 to 105 Hz due to increased elasticity of the MAM.

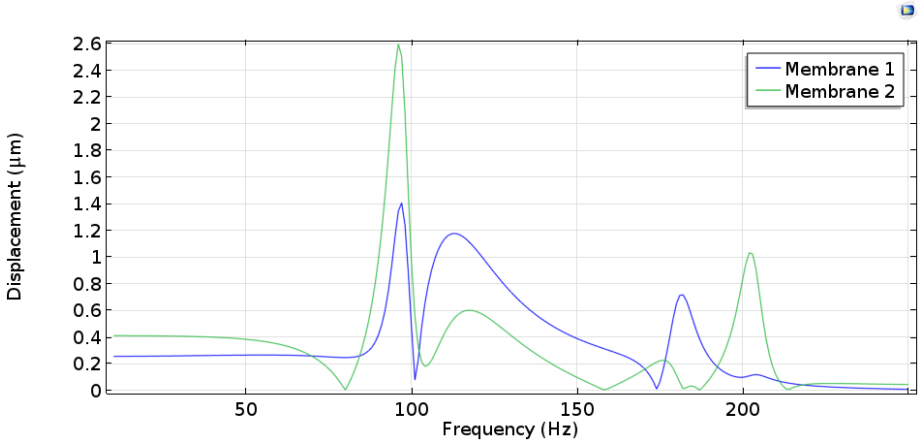

(a)

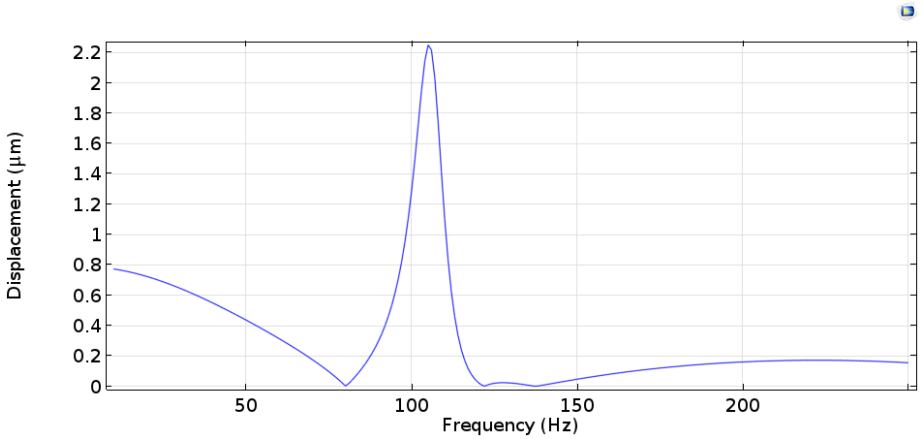

(b)

Figure 3.15: Displacement of membranes versus frequency of an incident wave (a) the two-port system and (b) the one-port system.

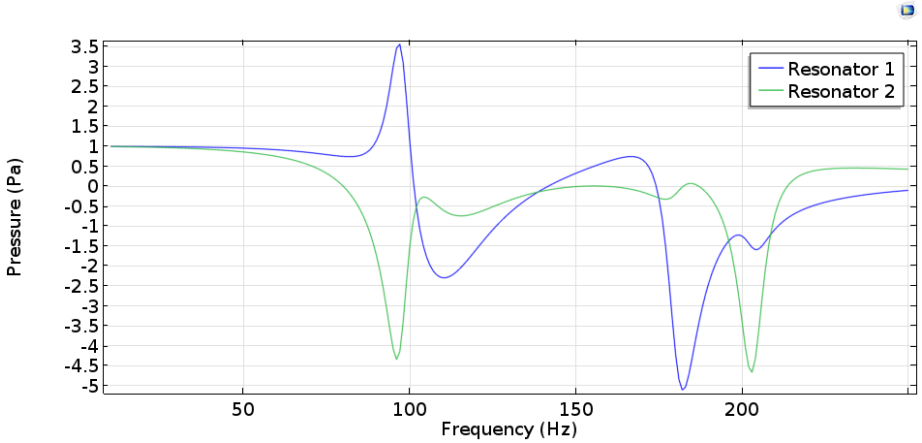

(a)

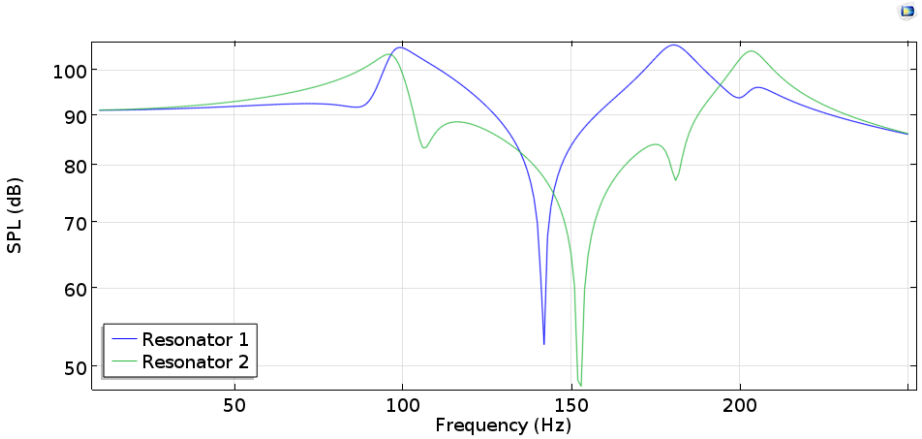

(b)

Figure 3.16: Acoustic properties of the HR-MAM couplings for two-port system. (a) acoustic pressure in the resonators, (b) SPL in the resonators.

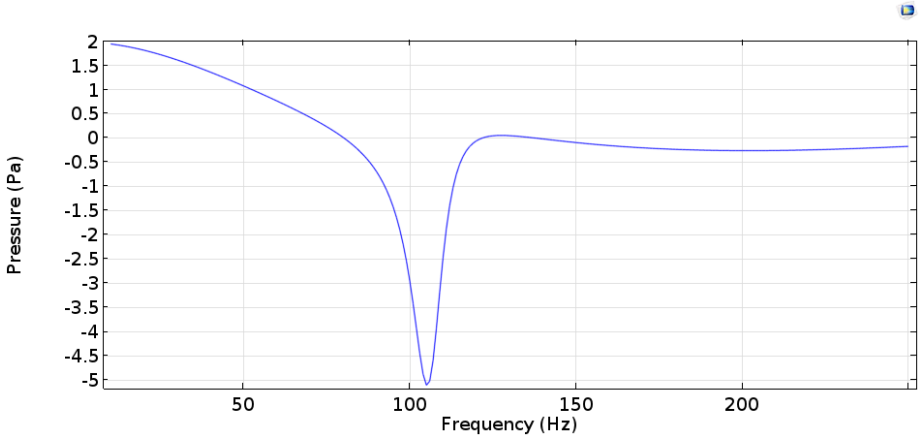

(a)

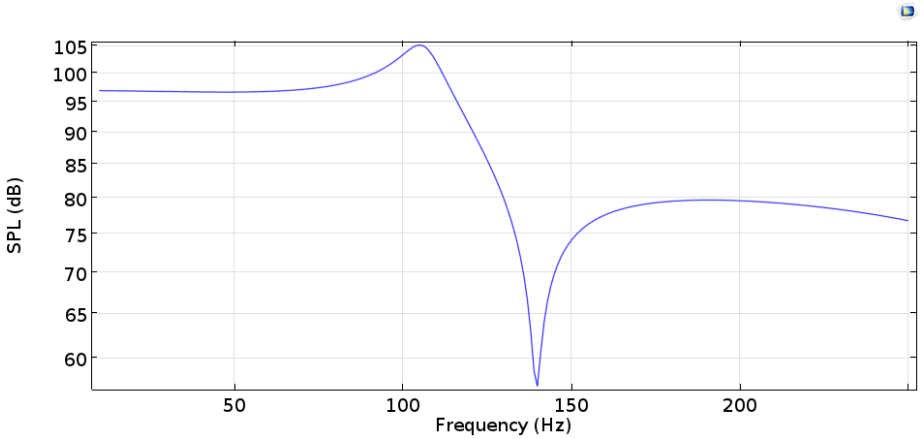

(b)

Figure 3.17: Acoustic properties of the HR-MAM couplings for the one-port system. (a) acoustic pressure in the resonator, (b) SPL in the resonator.

3.2.5 Structural - piezoelectric coupling

The structural dynamics and electrostatics is linked through the piezoelectric domain in the structural mechanics. The domain is charged through induced strains in the membrane. The coupling boundary is the entire membrane domain.

Electrical circuit

A scheme of an the electrical circuit describing induced electricity in the piezoelectric membrane is given in Figure 3.18. The voltage source, PVDF membrane is connected to a ground node through a resistance, creating a current.

(a) (b)

Figure 3.18: Electrical circuits in (a) the two-port and (b) the one-port systems.

The voltage sources are the PVDF films and the resistors in the open-end tube and closed-end tube, R_1, R_2 and R are the default resistors in COMSOL's electrical circuit physics node with a resistance of 1000 Ω.

3.3 Tuning the frequency with the membrane parameters

It can be seen from Equation (3.14) that the natural frequency of the membrane depends on the density(material), the thickness, the pretension and the radius. Even though altering the thickness and stress can be used to tune the membrane, it is infeasible to obtain a very thin or very thick membrane. Similarly, the tunability with the force is limited. The radius, on the other hand, has a larger effect on the vibration frequency. However, altering the radius also affects the frequency of the HR. Tuning the membrane with the attached mass is the most efficient and feasible option.

The thickness of the membrane, initial stress, radius of the attached mass and the thickness of the mass are the tuning parameters. There are PVDF films with 80μm, 100μm and 120μm commercially available so the thickness is selected among these options. The remaining parameters can be arbitrarily adjusted according to specific requirements.

The membrane and the mass parameters are used to tune the resonance to maximize the attenuation capability. It is explained in several studies given in Section 2 that with perfect coupling conditions, it is possible to achieve quasi-perfect(>95%) or even perfect(>99%) absorption rates [30] [20] . The goal is to achieve the critical coupling conditions.

For the two-port system, a slight difference of resonance frequency is required in the resonators so that the resonators are excited out of phase, resulting in a destructive interface on waves [20]. This means that two resonators will be partly de-tuned. For the one-port system, the distance from the resonator to the closed end of the tube is a function of wavelength(d $\approx \lambda/4$), meaning that with its adjustment, the length of the tube will also be modified. The tuning parameters and their admissible ranges are given in Table 3.9.

Membrane thickness	80 / 100 / 120	μm
Membrane tension	50 - 250	N/m
Mass radius	0.2 - 0.7	cm
Mass weight	0.1 - 1.5	g

Table 3.9: Tuning parameters for the MAM.

After the fine tuning of the MAMs is complete, the study suggests a maximum of 95% attenuation at 98 Hz for open-end tube and 99% attenuation for closed-end tube at 106 Hz with the selected parameters in Table 3.10. The outcomes of the study will be further discussed in the following section.

	Two-port		One-port
	MAM_1	MAM_2	
Membrane thickness [μm]	80	100	120
Membrane tension [N/m]	220	100	170
Mass radius [cm]	0.3	0.3	0.7
Mass weight [g]	1	0.5	0.1
1st eigenfrequency [Hz]	143	137	346

Table 3.10: Critical coupling conditions of the MAM's for open-end and closed-end tubes.

3.3.1 Mesh

To mesh the air inside the tube, the neck and the resonator, free tetrahedral elements are used. The mesh is calibrated for fluid dynamics in these parts. Approximately 10 - 12 nodes per wavelength are desired for an acoustic simulation and the shortest wavelength in these calculations is 36 cm, which corresponds to 950 Hz. The minimum element quality requirement, in this case, is 3 cm.

For the membrane, since out of plane deformation is the action of interest, the number of elements in the direction of normal is preferred. The faces of the membrane contain free triangular mesh to match with the tetrahedral mesh in the resonator and a sweep is done on the thickness of the membrane. Each element of the sweep has a length of 10μm.

The mass has triangular elements on its surfaces to match the resonator and the membrane but it has only a single element on its thickness direction. This is because the working frequency range is too low to cause deformation on the membrane, so it can be considered as a rigid body. To reduce the computational complexity, the mass is not meshed in its normal direction.

Among the three physic computations, pressure acoustics require the highest computational power. The degree of freedom in this problem, which is defined as the number of dependent variables multiplied by the number of nodes, is 117244, resulting in a computation time of approximately 20 minutes. However, the complexity increases severely when the problem is coupled with solid mechanics and electrostatics. The coupled model has 1450156 degrees of freedom, causing a computation time of approximately 9 hours.

4. Results and Discussions

4.1 Parametric study

The alteration of the parameters of the membrane enabled the de-tuning of the two resonators, resulting in enhanced absorption. Yet, de-tuning a resonator also affects the frequency of the absorption peak. The dependency of the peak frequency on tuning parameters is investigated and represented below.

Figure 4.1a demonstrates the dependency of the absorption peak frequency on membrane tension and the radius of the attached mass. The weight of the mass is kept constant at 0.1 g, where the highest absorption is observed. Figure 4.1b demonstrates a similar result by keeping the radius constant at 0.7 cm and altering the weight of the attached mass and Figure 4.1c keeps the pretension at 170 N/m. The results are compatible with the fact that the resonance frequency of a system depends on the stiffness and the inertia. Increasing the membrane tension increased the frequency in both cases due to the increased stiffness. Increasing the weight of the mass increases the inertia of the membrane, thus, reducing the frequency.

4.2 Flow properties

4.2.1 Pressure distribution

The pressure distributions inside the open-end tube at the frequency of peak of attenuation and at the frequency of minimum point of attenuation are given in Figures 4.2a and 4.2b.

First, in the two-port system, note that the resonators are out of phase at the maximum attenuation frequency. The resonator on the inlet side has a maximum pressure while the resonator on the outlet side has a minimum pressure. As mentioned before, the increased attenuation capacity is observed due to this phase difference in the operation of the resonators. The pressure inside the tube is gradually decreasing except for the discrepancies caused by the resonators. When the pressure inside the resonators are both at a minimum point, which also indicates the in-phase operation, the attenuation reaches the minimum point at 150 Hz as in Figure 4.6.

Since the one-port system has a single resonator and a closed end, the pressure distribution is slightly different than for the two-port system (Figure 4.3). At the maximum of attenuation, the resonator has a negative maximum and at the dip of attenuation the resonator is a part of the gradual descent of pressure within the tube.

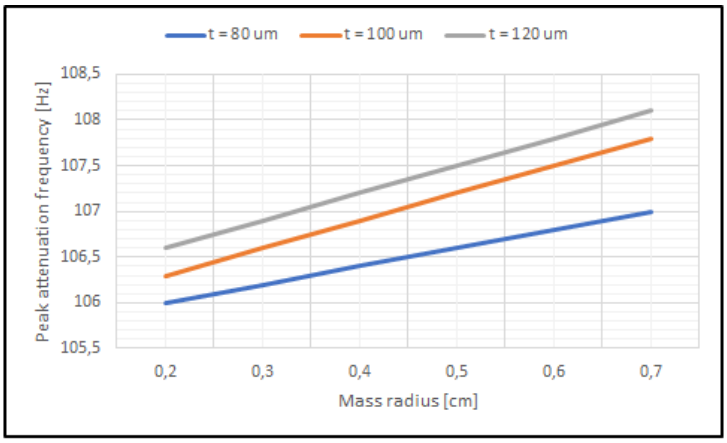

(a)

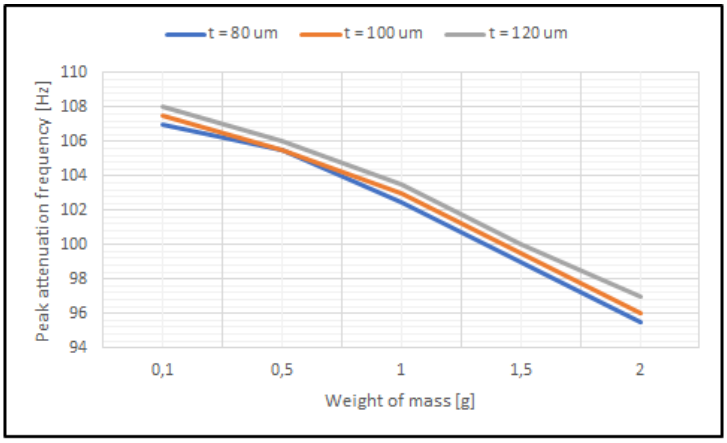

(b)

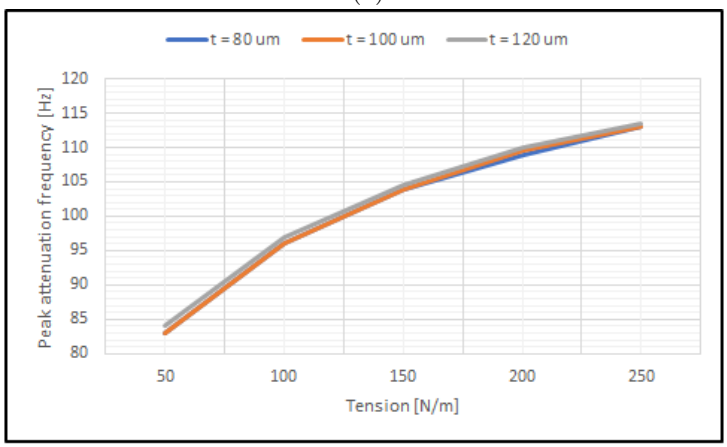

(c)

Figure 4.1: The dependency of the peak attenuation frequency to (a) radius of the mass, (b) weight of the mass and (c) tension on the membrane.

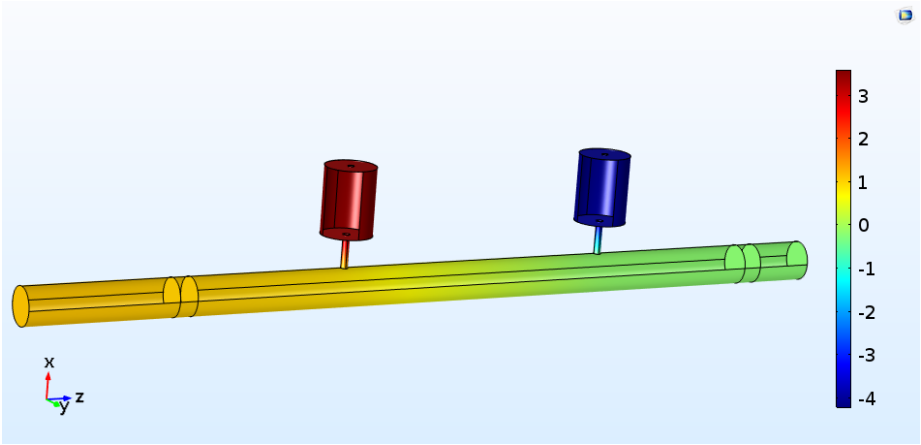

(a)

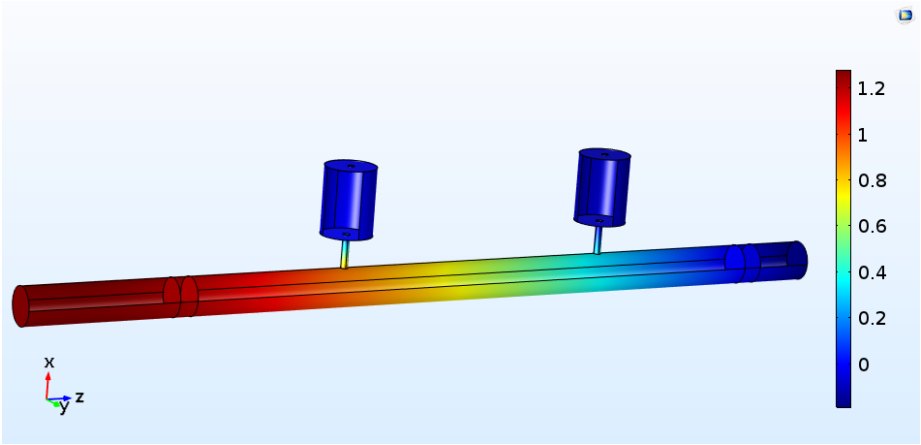

(b)

Figure 4.2: Pressure distributions in the two-port system at (a) maximum attenuation frequency, 97 Hz and (b) minimum attenuation frequency, 150 Hz.

4.2.2 Flow velocity

The final flow property under consideration is the velocity of the air inside the tube and around the area of the HRs. Figures 4.4 and 4.5 represent the direction of the flow at the frequency of peak of attenuation.

As explained in Section 4.2.1, the first resonator (left) has a positive pressure while the second resonator (right) has a negative pressure inside the cavity at the peak attenuation frequency. This leads to the airflow out of the second resonator and inside the first resonator, as can be seen in Figure 4.4a. The flow direction inside the waveguide is from the second resonator to the first resonator, which can also be seen in Figure 4.4b.

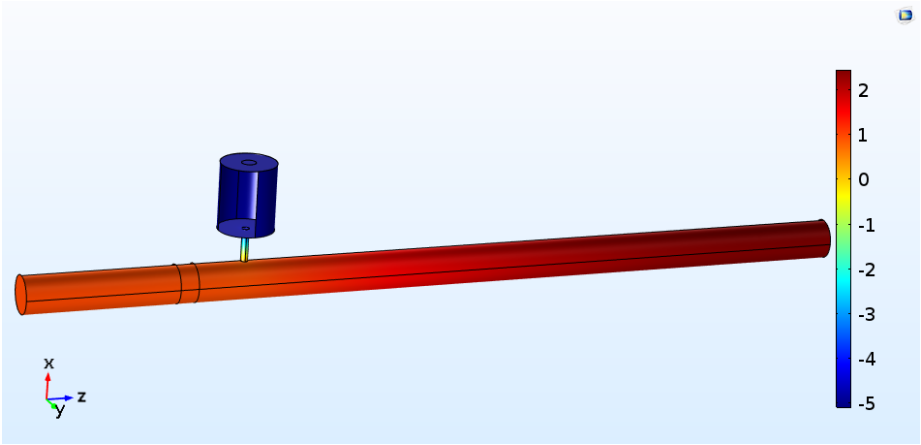

(a)

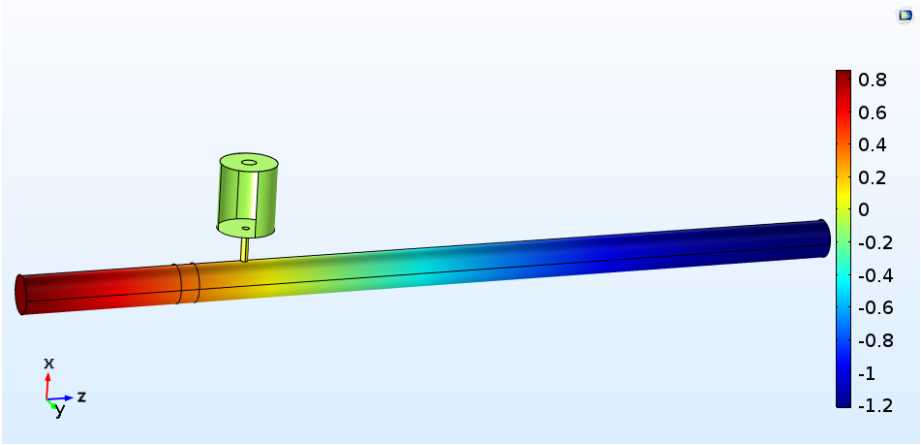

(b)

Figure 4.3: Pressure distributions in the one-port system (a) maximum attenuation frequency, 106 Hz and (b) minimum attenuation frequency, 150 Hz.

Similar to the open-end tube, the pressure inside the resonator for closed-end tube at the peak attenuation frequency has a negative value, leading the flow to point towards the resonator. Since the right hand side of the resonator is closed, the velocity at that point is zero.

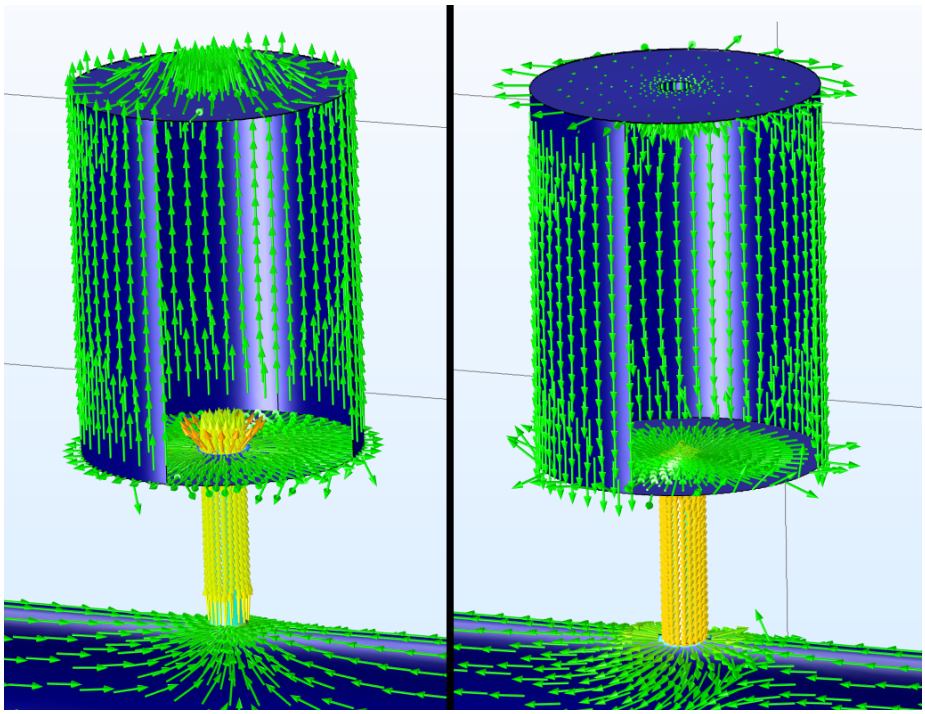

(a)

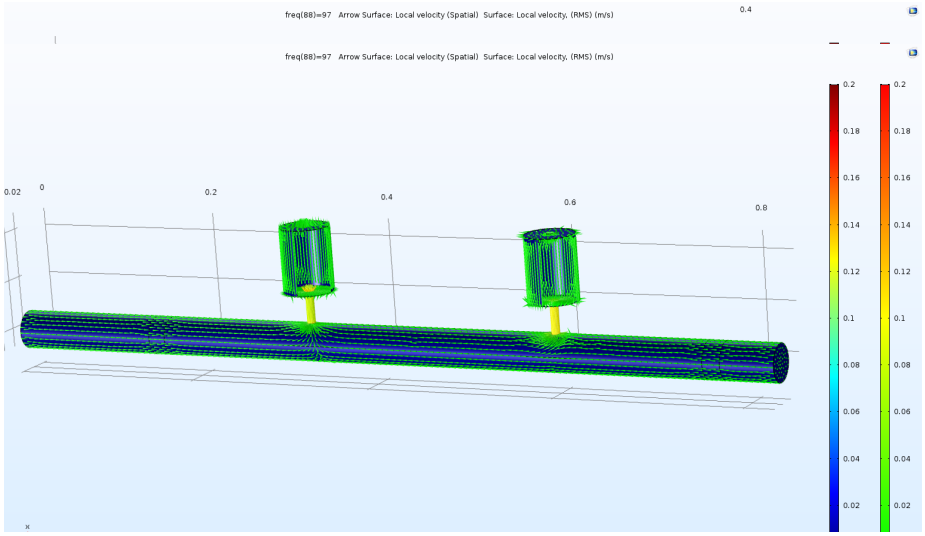

(b)

Figure 4.4: Velocity distribution in (a) the resonators and (b) in the open-end tube.

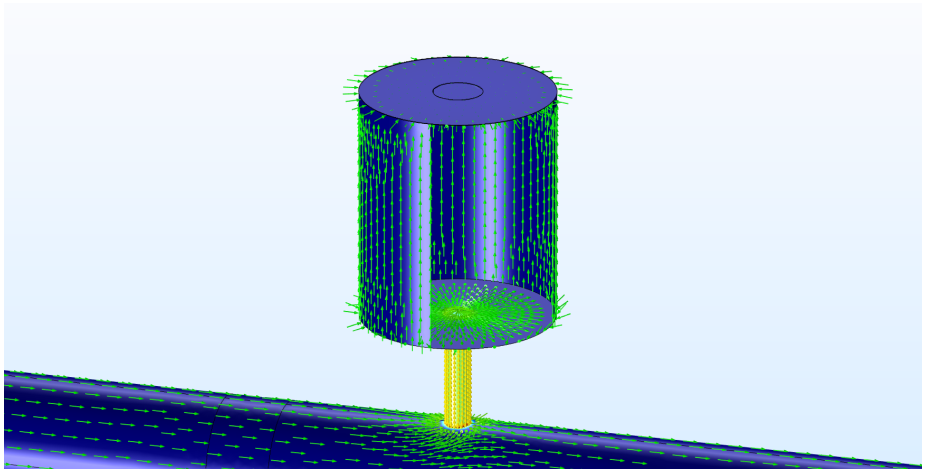

(a) .

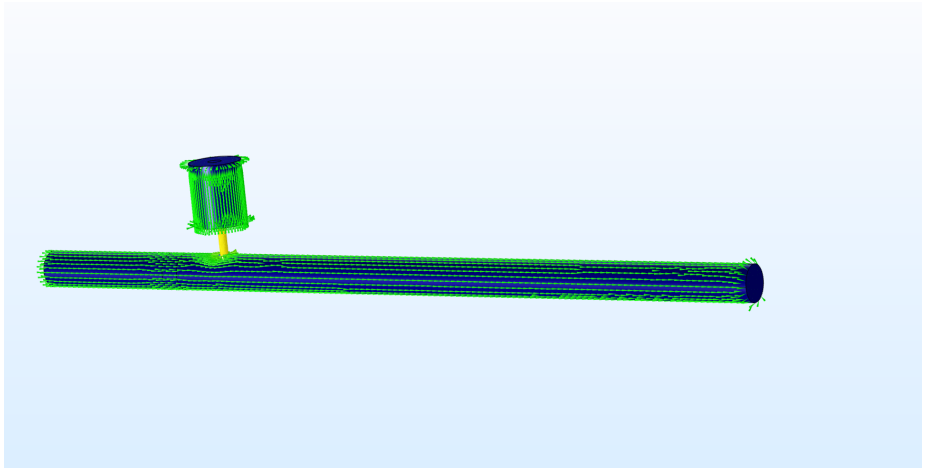

(b) .

Figure 4.5: Velocity distribution in (a) the resonators and (b) in the closed-end tube.

4.3 Noise reduction

The numerical data reveals excellent noise reduction for both two-port and one-port systems. Two-port system exhibits approximately 95% attenuation ($\alpha \approx 0.95$), which is addressed as "quasi-perfect absorption" while the one-port system has even better absorption over 99% ($\alpha > 0.99$). Figure 4.6 represents the transmission(T), reflection(R) and attenuation(A) coefficients of the two-port system. For the one-port system, since the transmission is not possible, only reflection(R) and attenuation(A) coefficients are calculated. Those are given in figure 4.7.

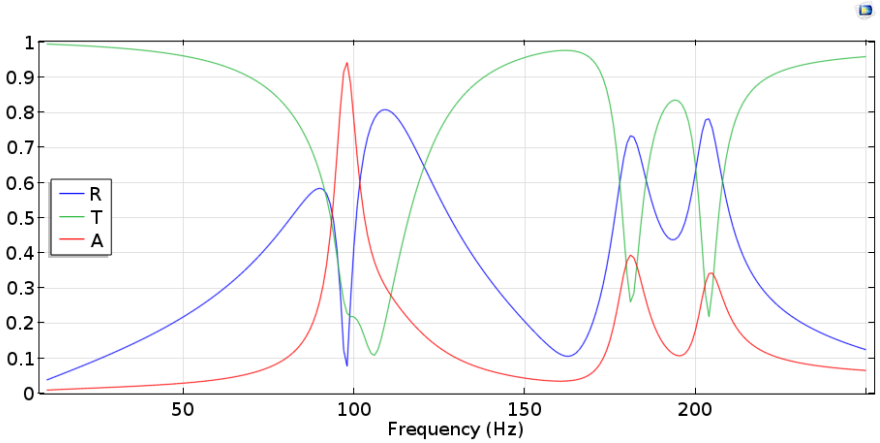

Figure 4.6: R, T and A coefficients of the two-port system.

The absorption coefficient at the resonance frequency is 0.95, indicating the quasi-perfect absorption. While the bandwidth of attenuation($\Delta f_{0.5}$) is 9.5 Hz.

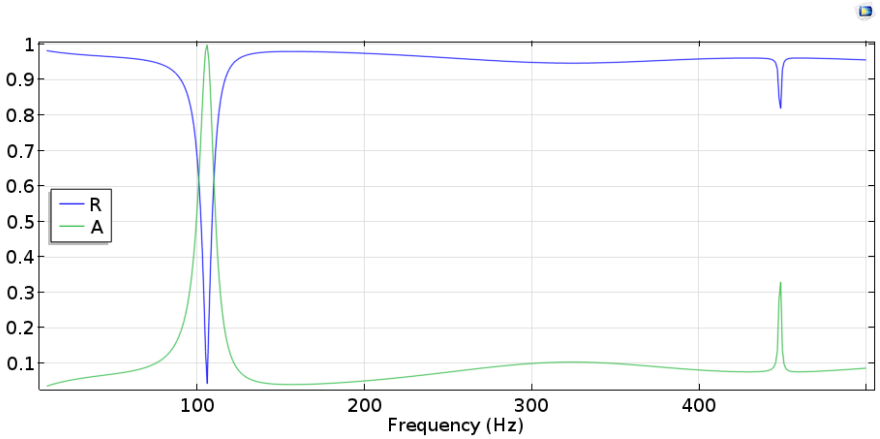

Figure 4.7: R and A coefficients of the one-port system.

The attenuation of the one-port system is over 0.99, indicating perfect absorption. The bandwidth in this case is $\Delta f_{0.5} = 11.6$ Hz.

Transmission loss is defined as the decrease of the energy of a wave in a certain domain [6]. It is used to define the isolation performance of an insulator or in this case, the performance of the two-port system. The transmission losses for the two-port system is given in Figure 4.8. Since there is no acoustic outlet for the one-port system, TL can not be calculated. For the two-port system, a TL over 40 dB was calculated. In addition to the resonance frequency of the resonator, two other smaller TL peaks of approximately 25 dB are observed at 181 Hz and 204 Hz, at the higher modes of the membrane, enabling noise reduction at a larger frequency range.

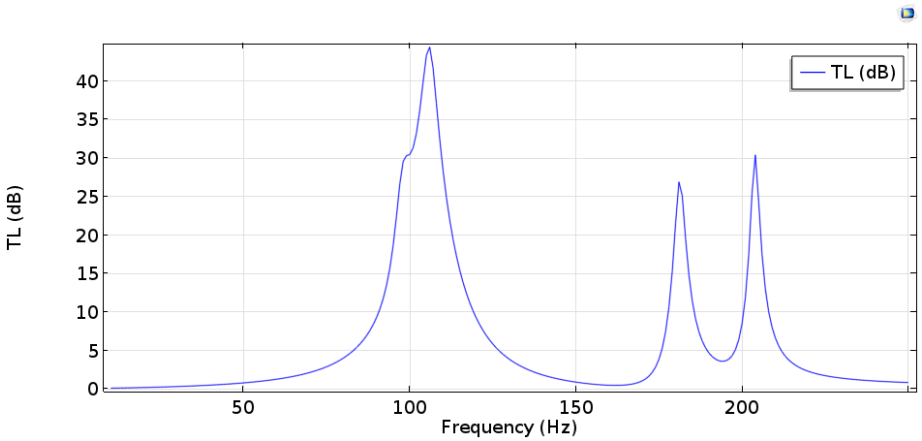

Figure 4.8: Transmission loss of the two-port system.

4.4 Energy harvesting

The energy output of the system is given in Figures 4.9 and 4.10 for two-port and one-port systems, as well as the voltage output in Figures 4.9b and 4.10b. It is obvious that the energy output is on a nanoscale, which could be considered "inefficient" for such a design. However, it must also be noted that the focus of this research was not on the optimization of the harvesting mechanism. The results indicate that it is possible to generate acoustic energy into electricity by the means of the proposed systems, meaning that the research goal is sufficiently reached.

Even though the attenuation capacity of the one-port system is slightly higher, the energy output for the two-port system is similarly higher than that for the one-port system. Since the radius for the PVDF film is the same in all resonators, the two-port system has two times more piezoelectric material since it has two resonators and films attached, which makes it reasonable to conclude that for energy harvesting purposes, the two-port system is more efficient.

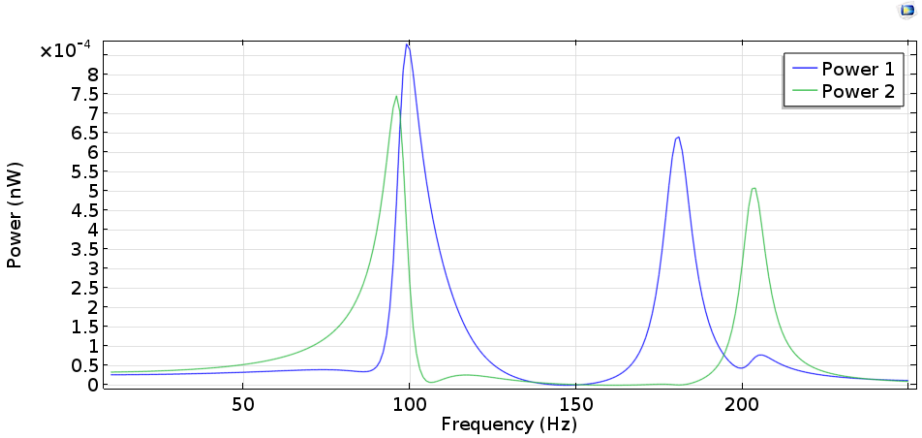

(a)

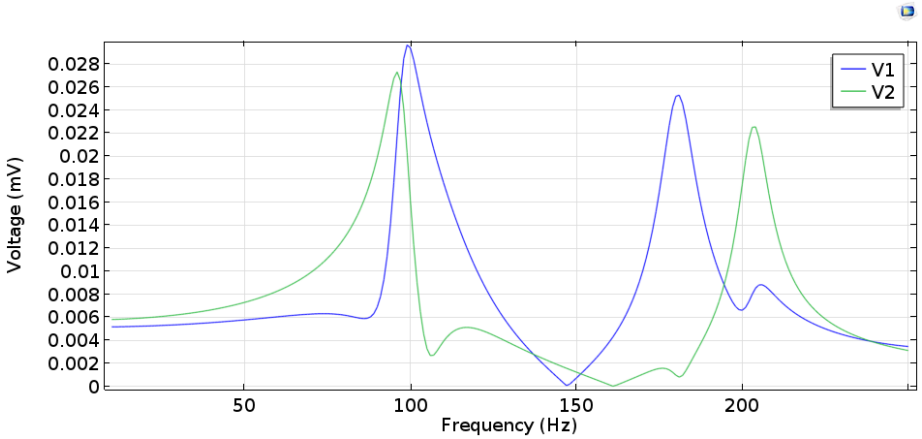

(b)

Figure 4.9: (a) The power output and (b) the voltage output of the two-port system.

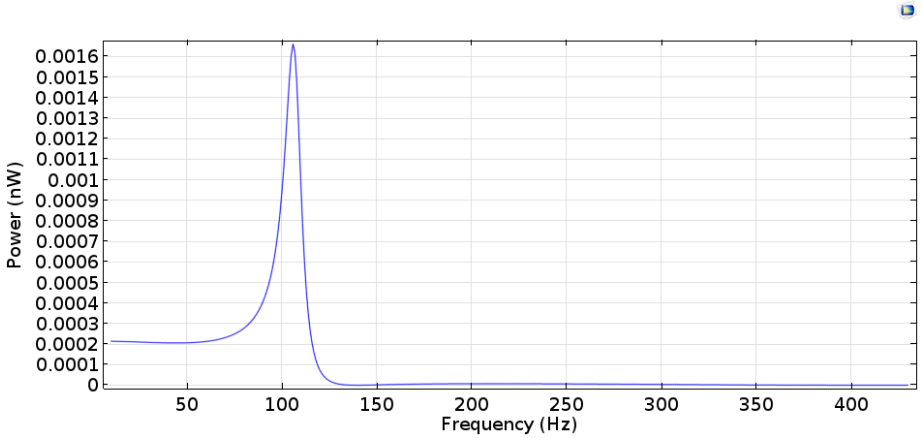

(a)

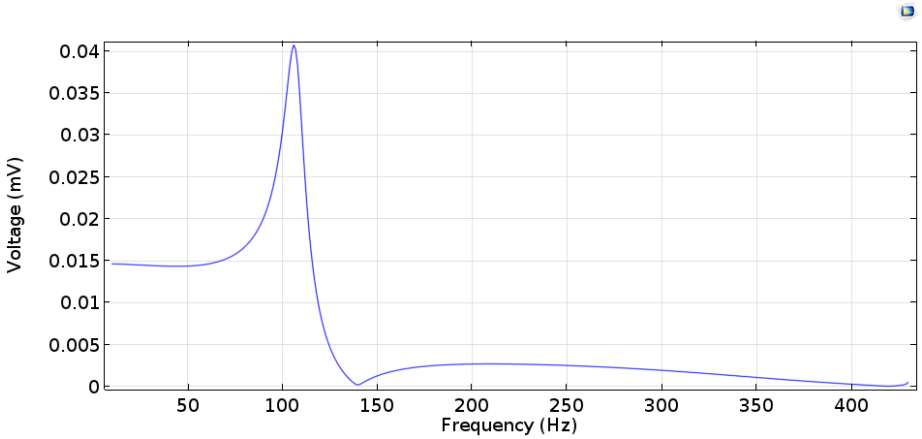

(b)

Figure 4.10: (a) The power output and (b) the voltage output of the one-port system.

5. Conclusions

The study aimed to investigate the possibility to attenuate the sound on a sub-wavelength scale while generating energy. The method to conduct this research was to utilize a Helmholtz resonator coupled with a membrane-type acoustic metamaterial to adjust the characteristics of the resonator according to the requirements. The analysis mentioned in Section 3 provided sufficient answer to the main research question stated as;

"How can membrane-type metamaterials be utilized to tune a structure with the purpose of concurrently attenuate the noise and generate energy from acoustic waves?"

The four sub-questions derived from the main research question are explained and answered in this section. The decomposition of the main problem is expressed as following:

1. **How does the tuning of the resonators affect the attenuation frequency?**

   The answer to the first question was investigated through a parametric study where the four membrane parameters; thickness, tension, weight of the mass and radius of the mass; are tested through a range to determine the effect on the peak attenuation frequency and maximum attenuation rate.

   By tuning the MAM, it is possible to tune the frequency response of the resonator up to 35% of its resonance frequency in the given range. Increasing the stiffness of the system through the tuning parameters such as increasing the tension or the thickness of the membrane leads to an increase in the resonance frequency. Increasing the inertia of the system by increasing the mass weight or radius decreases the frequency [43].

2. **How does the configuration of the HR affect the design and performance?**

   Two alternative approaches were studied numerically: a one-port system with a single resonance and a closed-end tube and a two-port system with a dual resonance and an open-end tube. For the dual-resonance system, the distance between two resonators causes an extra degree of freedom to the design process of the tube. For the closed-end version, the distance between the resonator and the reflective surface on the closed end is a function of frequency, thus, it is not considered as a design parameter. Adjusting the length and the diameter of the tube was also a requirement to ensure that the structure is capable of attenuating the desired wavelength.

When the tube has a closed-end, total absorption can be achieved when the backward reflecting waves from the end of the tube creates a destructive interface with the forward radiating waves from the resonator [20]. To reach this condition, the distance should be arranged to be a quarter of the wavelength of the resonance frequency, $d \approx \lambda/4$. For the open-end tube, the requirement for PA is to keep the distance between two resonators smaller than the quarter of the wavelength, $d < \lambda/4$. The closed-end tube performed slightly better(4% higher absorption) than the open-end tube for sound attenuation. The length and diameter of the tube were optimized to maximize the attenuation rate. Even though reducing the size of the tube was intended, too much reduction results in the incapability of successfully attenuating waves with a large wavelength. On the energy generation side, the open-end tube performed better than the closed-end tube, which was expected since the closed-end tube has a single PVDF film that converts acoustic energy into electricity while the open-end tube has two.

3. **Does the energy harvesting process affect the efficiency of the noise reduction performance?**

   The study started with a validation step where designs from published studies were used as starting points to confirm the accuracy of the numerical models in this study. Therefore, the initial models aimed only to investigate the acoustic properties. These models are then adjusted by changing the dimensions and finally coupled with the membrane and the energy harvesting mechanism.

   Both for the two-port system and one-port system, over 0.95 absorptions were observed, meaning that coupling the HR with the membrane and energy harvesting mechanism did not cause a significant reduction in the noise reduction performance.

4. **What is the effect of the introduced elasticity by the membrane on the flow characteristics within the impedance tube?**

   The top surface of the HR was replaced by a MAM with a piezoelectric material, increasing the elasticity of the resonator. Since Helmholtz resonance is basically a mass-spring system with the air inside the cavity acting as the spring and the air inside the neck as the mass, reducing the rigidity results in a decrease of the resonance frequency. On contrary, the pressure field inside the resonator causes an increased force on the membrane, increasing its stiffness. The eigenfrequencies of the membrane increase due to this effect. The difference between the separate models and the coupled model is also observable in the attenuation. The peak frequency of attenuation is decreased for the coupled model, which supports the research as the intention was to attenuate wavelengths much larger than the dimensions of the structure. With the final configuration, the wavelength of maximum attenuation is 50 times larger than the length of the resonator and 4.5 times larger than the total length of the impedance tube.

5.1 Limitations of the study

Even though the study relies mostly on numerical analysis, several assumptions were made to simplify the computation. The sound hard boundaries at the walls of the impedance tube and the resonator assume that the wave propagation speed at the wall(and the solid material of the wall) is 0. It was not covered in this study how much this assumption affects the results.

Experimentation is usually a crucial part of acoustic studies. Although the results from the numerical analysis appear to be solid, a validation through experiment would strengthen the concluding statement.

5.2 Future research

The study provided insight into the acoustic properties of a MAM coupled HR while optimizing the tuning parameters for maximum attenuation. Yet there still remain several aspects that can be done in the following studies to enhance the outcomes of this research.

To start with, as mentioned before, the interest of this study was limited to the sound attenuation performance of the proposed system. However, the optimization of the energy harvesting mechanism stands as a solid research topic. The material used in this study as the piezoelectric film was Polyvinylidene fluoride and the material properties were taken as default from COMSOL's interface. However, it is possible to engineer the material according to this specific purpose to achieve maximum energy generation. Moreover, the MAM-HR coupling can be tuned for energy harvesting purposes. The HR resonance frequency for the current configuration is slightly lower than the eigenfrequency of the membrane to achieve maximum attenuation. Tuning the two frequencies to exactly match to increase the displacement on the membrane would provide maximum energy harvesting. An optimization between two desired properties(attenuation and generation) could be another opportunity.

The study focused on single resonance and dual resonance resonators, however, the number of resonators on an impedance tube is not limited. It was explained in Section 2 that HR's have a narrow band of attenuation and demonstrated in Section 4 that the two-resonator model provided higher energy generation because it had two energy harvesters instead of one in the single-resonance resonator. Similarly, the number of resonators could be increased for higher energy harvesting and also for a broader band of attenuation.

The HR frequency and MAM frequency in the coupled model deviates from the separate analysis as shown in Section 3. The increased elasticity in the resonator causes the resonance frequency to drop and the increased pressure on the membrane causes the vibration frequency to increase. The analytical model for this coupling effect on frequencies can be a challenging subject to investigate.I

Bibliography

[1] Vassos Achilleos, Olivier Richoux, and Georgios Theocharis. Coherent perfect absorption induced by the nonlinearity of a helmholtz resonator. *The Journal of the Acoustical Society of America*, 140:EL95, 2016.

[2] Standard test method for normal incidence determination of porous material acoustical properties based on the transfer matrix method. Standard ASTM E2611 - 17, American Society for Testing and Materials, Pennsylvania, USA, 2019.

[3] Allan Bower. In *Applied Mechanics of Solids*, 2009.

[4] Daniel Brooke, Olga Umnova, Philippe Leclaire, and Thomas Dupont. Acoustic metamaterial for low frequency sound absorption in linear and nonlinear regimes. *Journal of Sound and Vibration*, 485:115585, 2020.

[5] Fabio Cosmo, Marco Laudato, and Mario Spagnuolo. *Acoustic Metamaterials Based on Local Resonances: Homogenization, Optimization and Applications*, pages 247–274. 2018.

[6] Malcolm Crocker and Scott Sommerfeldt. Handbook of noise and vibration control. *The Journal of the Acoustical Society of America*, 124:1898, 2008.

[7] Benjamin Crowell. *Simple Nature*, page 344. 2005.

[8] Shichao Cui and Ryan Harne. Soft materials with broadband and near-total absorption of sound. *Physical Review Applied*, 12:064059, 2019.

[9] Steven Cummer, Johan Christensen, and Andrea Alú. Controlling sound with acoustic metamaterials. *Nature Reviews Materials*, 1(3):16001, 2016.

[10] Peng Dong-Li, Hu Peng, and Zhu Bei-Li. The modified method of measuring the complex transmission coefficient of multilayer acoustical panel in impedance tube. *Applied Acoustics*, 69(12):1240–1248, 2008.

[11] Abhishek Gautam, Alper Celik, and Mahdi Azarpeyvand. An experimental and numerical study on the effect of spacing between two helmholtz resonators. *Acoustics*, 3(1):97–117, 2021.

[12] Dan Givoli and Beny Neta. High-order non-reflecting boundary scheme for time-dependent waves. *Journal of Computational Physics*, 186(1):24–46, 2003.

[13] Chad Greene, Theodore Argo, and Preston Wilson. A helmholtz resonator experiment for the listen up project. *The Journal of the Acoustical Society of America*, 124:2568, 2008.

[14] Jingwen Guo. Low-frequency sound absorber based on checkerboard helmholtz resonators with different extended necks. Institute of Noise Control Engineering, 2019.

[15] Stephen Horowitz, Mark Sheplak, Louis Cattafesta, and Toshikazu Nishida. A mems acoustic energy harvester. *Journal of Micromechanics and Microengineering*, 16(9), 2006.

[16] Noé Jiménez, Vicent Romero-García, Vincent Pagneux, and Jean-Philippe Groby. Rainbow-trapping absorbers: Broadband, perfect and asymmetric sound absorption by subwavelength panels for transmission problems. *Scientific Reports*, 7(13595):1, 2017.

[17] Rakhesh Singh Kshetrimayum. A brief intro to metamaterials. *IEEE Potentials*, 23(5):44–46, 2005.

[18] Felix Langfeldt, Wolfgang Gleine, and Otto von Estorff. Analytical model for low-frequency transmission loss calculation of membranes loaded with arbitrarily shaped masses. *Journal of Sound and Vibration*, 349:315–329, 2015.

[19] Kong Ju Bock Lee, Myoung Ki Jung, and Sam Lee. Highly tunable acoustic metamaterials based on a resonant tubular array. *Physical Review B*, 86(184302), 2012.

[20] Taehwa Lee, Tsuyoshi Nomura, and Hideo Iizuka. Damped resonance for broadband acoustic absorption in one-port and two-port systems. *Scientific Reports*, 9:13077, 2019.

[21] Bin Li, Andrew Laviage, Jeong Ho You, and Yong-Joe Kim. Harvesting low-frequency acoustic energy using quarter-wavelength straight-tube acoustic resonator. *Applied Acoustics*, 74(11):1271–1278, 2013.

[22] Junfei Li, Xiaoming Zhou, Guoliang Huang, and Gengkai Hu. Acoustic metamaterials capable of both sound insulation and energy harvesting. *Smart Materials and Structures*, 25(4):045013, 2016.

[23] Johan Liljencrants. End correction at a flue pipe mouth, 2006. http://www.fonema.se/mouthcorr/mouthcorr.htm, accessed: 18.05.2021.

[24] Reece Lincoln, Fabrizio Scarpa, Valeska Ting, and Richard Trask. Multifunctional composites: a metamaterial perspective. *Multifunctional Materials*, 2(4):043001, 2019.

[25] Guang-Sheng Liu, Yao-Yin Peng, Ming-Hao Liu, Xin-Ye Zou, and Jian-Chun Cheng. Broadband acoustic energy harvesting metasurface with coupled helmholtz resonators. *Applied Physics Letters*, 113:153503, 2018.

[26] Yang Liu and Jingtao Du. Vibroacoustic characteristics and sound attenuation analyses of a duct–membrane system coupled with strip masses. *Journal of Vibration and Control*, 25:107754631987345, 2019.

[27] Zhengyou Liu, Xixiang Zhang, Yiwei Mao, Yan Yang Zhu, Zhiyu Yang, Che Ting Chan, and Ping Sheng. Locally resonant sonic materials. *Science*, 289(5485):1734–1736, 2000.

[28] Zhenbo Lu, Xiang Yu, Siu-Kit Lau, Boo Cheong Khoo, and Fangsen Cui. Membrane-type acoustic metamaterial with eccentric masses for broadband sound isolation. *Applied Acoustics*, 157:107003, 2020.

[29] Rosa Martinez-Sala, Jose Sancho, Juan Sánchez-Pérez, Vicente Gomez, Jaime Llinares, and Francisco Meseguer. Sound attenuation by sculpture. *Nature*, 378(6554):241–241, 1995.

[30] Aurelien Merkel, Georgios Theocharis, Olivier Richoux, Vicent Romero-García, and Vincent Pagneux. Control of acoustic absorption in one-dimensional scattering by resonant scatterers. *Applied Physics Letters*, 107:244102, 2015.

[31] Yongzhen Mi and Xiang Yu. Attenuation of low-frequency sound in u-shaped duct with membrane coupled acoustic resonator: Modeling and analysis. *Journal of Sound and Vibration*, 489:115679, 2020.

[32] Maxim Mironov, Alexander Komkin, and Aleksei Bykov. Sound absorption by a helmholtz resonator. *Acoustical Physics*, 63:385–392, 2017.

[33] Minu Pillai and Ezhilarasi Deenadayalan. Acoustic energy harvesting using helmholtz resonator with tapered neck. 2014.

[34] Jacek Pniewski, Wladyslaw Marek Saj, Tomasz Antosiewicz, and Tomasz Szoplik. Metamaterials: composite materials with unnatural electromagnetic properties. In Anton Štrba, Dagmar Senderákova, and Miroslav Hrabovský, editors, *14th Slovak-Czech-Polish Optical Conference on Wave and Quantum Aspects of Contemporary Optics*, volume 5945, pages 424 – 432. International Society for Optics and Photonics, SPIE, 2006.

[35] V. Romero-García, G. Theocharis, O. Richoux, A. Merkel, V. Tournat, and V. Pagneux. Perfect and broadband acoustic absorption by critically coupled sub-wavelength resonators. *Scientific Reports*, 6(1):19519, 2016.

[36] Occupational Safety and Health Act. Osha standard 1910.95, 1970. https://www.osha.gov/laws-regs/regulations/standardnumber/1910/1910.95, accessed: 28.02.2021.

[37] Yacoubou Salissou and Raymond Panneton. A general wave decomposition formula for the measurement of normal incidence sound transmission loss in impedance tube. *The Journal of the Acoustical Society of America*, 125:2083–90, 2009.

[38] Michael Stinson. The propagation of plane sound waves in narrow and wide circular tubes, and generalization to uniform tubes of arbitrary cross-sectional shape. *Journal of the Acoustical Society of America*, 89:550–558, 1991.

[39] Viktor Veselago. The electrodynamics of substances with simultaneously negative values of ϵ and μ. *Soviet Physics Uspekhi*, 10(4):509–514, 1968.

[40] Davide Vigé. Vehicle interior noise refinement – cabin sound package design and development. In Xu Wang, editor, *Vehicle Noise and Vibration Refinement*, pages 286–317. Woodhead Publishing, 2010.

[41] Yuan Wang, Xin Zhu, Tingsheng Zhang, Shehar Bano, Hongye Pan, Lingfei Qi, Zutao Zhang, and Yanping Yuan. A renewable low-frequency acoustic energy harvesting noise barrier for high-speed railways using a helmholtz resonator and a pvdf film. *Applied Energy*, 230:52–61, 2018.

[42] Min Yang, Chong Meng, Caixing Fu, Yong Li, Zhiyu Yang, and Ping Sheng. Subwavelength total acoustic absorption with degenerate resonators. *Applied Physics Letters*, 107:104104, 2015.

[43] Chen Yangyang, Xiaoming Zhou, Gengkai Hu, Chin-Teh Sun, and Guoliang Huang. Analytical coupled vibroacoustic modeling of membrane-type acoustic metamaterials: Membrane model. *The Journal of the Acoustical Society of America*, 136, 2013.